

## **Response to Anonymous Referee #1 comments to paper “Tropospheric vertical column densities of NO<sub>2</sub> over managed dryland ecosystems (Xinjiang, P. R. China): MAX-DOAS measurements vs. 3D dispersion model simulations based on laboratory derived NO emission from soil samples”**

The authors would like to thank Anonymous Referee #1 for his/her constructive comments.

### **Specific comments:**

- 1. Page 19361, line 15: please add “e.g.” in the list of references.**
  - *“e.g.” have been added in the revised MS.*
- 2. Page 19362, line 27: a more recent reference, if it is available, would be beneficial.**
  - *In the revised MS, the reference “World Map of the Koeppen-Geiger classification updated” by Kottek et al (2006) will be used.*
- 3. Page 19363, Line 26: add “nm” after “420-450”.**
  - *“nm” have been added.*
- 4. Page 19365, line 2: define what the “m a.gr.” stands for, is this meters above ground?**
  - *Yes*
- 5. Page 19366, line 16: Is the “59.8 dS m<sup>-1</sup>” the right value for natural forests? Please check.**
  - *Yes, it is the right value for the natural forest. The natural forest in study area are associated with mainly Tamarix species and P. euphratica and they depends on groundwater. The plant species of Tamarix widespread in salty and sandy land in arid area. Natural forest, so called by the local people because the unique tree species makes it possible to reverse environmental degradation.*
- 6. Page 19366, line 17: what “TDR” and “FDR” stand for?**
  - *TDR (Time-Domain-Reflectometry) and FDR (Frequent Domain Reflectometry) have been added.*
- 7. Page 19366, line 25: please explain the “pF 4.2”.**
  - *The relation between soil moisture and soil moisture content expressed as pF curve (soil moisture retention curve). When the soil becomes dry the soil moisture content reached the minimum value then the soil is at permanent wilting point or has a pF=4.2. This means, that the theta min is equal to the permanent wilting point.*
- 8. Page 19378, section 3.3: what about the errors in both measured and simulated NO<sub>2</sub> VCDs? Please discuss further the results of Figure 5.**
  - *We would like to thank Anonymous Referee #1 for this suggestion. And we assume that the referee #1 wanted to say the Figure 7 (in MS version Fig. 8). This sentence has been added in revised MS “Both measured and simulated NO<sub>2</sub> VSDs in Figure 7 have with an average root mean square (RMS) error between the measured and simulated values of approx. 5-15% ”*
- 9. Page 19380, Conclusions: I suggest rewriting the first paragraph. I found it too difficult to follow its structure.**
  - *We acknowledge the suggestions of Anonymous Referee #1.*
- 10. Page 19380, lines 22-24: please give a reference (or source) for the central European wheat field NO fluxes values.**
  - *The related references have been added in MS (Yamulki et al. 1995; Stohl et al. 1996; etc.)*
- 11. Page 19393, Figure 6: at the color scale the white box corresponds to values greater than 10000. Shouldn't it be less than 10000? Please check it.**

- *The authors like to thank Anonymous Referee #1 for his comment concerning our typing mistake. There was a simple typo (“>” instead of “<”).*

**Technical comments:**

- 1. Abstract, line 15: please add “(3-D)” after the “three dimensional”**
  - *“three dimensional” has been added in revised MS.*
- 2. Page 19363, line 3: please add the word “is” after “mean wind speed”**
  - *“is” has been added in revised MS.*
- 3. Page 19366, line 28: please remove “there”**
  - *“there” has been removed in revised MS.*
- 4. Page 19376, line 6: please delete “net” before “NO”**
  - *“net” has been removed in revised MS.*
- 5. Page 19378, lines 15: please delete “the” after “NO”**
  - *“the” has been removed in revised MS.*

## **Response to Anonymous Referee #2 comments to paper “Tropospheric vertical column densities of NO<sub>2</sub> over managed dryland ecosystems (Xinjiang, P. R. China): MAX-DOAS measurements vs. 3D dispersion model simulations based on laboratory derived NO emission from soil samples”**

The authors would like to thank Anonymous Referee #2 for his/her constructive comments.

### **Response to the comments listed as Major issues:**

**P19372, L5: it is not clear why the LASAT model is ‘state-of-art’. From the description, it appears that chemistry is missing from the model, so that temporal evolution of the chemically active NO-species is difficult to track. Furthermore, it is unclear how pixel cross-talk, or advection, in the model (highly relevant with model resolution of 30 m) is described. The authors should improve the description of these issues.**

*The term “state-of-the-art” has been chosen since (a) LASAT is one of those air-pollution-transport-dispersion models of air-pollution which is (in Germany ) officially licensed for legal use of environmental issues, and (b) among comparable micro-scale (e.g. street canyons) transport-dispersion models LASAT considers at least chemical transformations of 1<sup>st</sup> order and keeps nonetheless truly operational. Being a transport-dispersion-model, LASAT basically considers advection (“pixel cross-talk”) applying the 3D-continuity equation for any chosen tracer; the interested reader is referred to the cited reference (German VDI Guidelines VDI3945, part 3; cf. Janicke Consulting, 2011).*

**P19372, L5: Calculation of concentration of NO<sub>2</sub> from the photochemical equilibrium between NO and O<sub>3</sub> is in principle feasible. However, O<sub>3</sub> concentration increase with altitude, and J(NO<sub>2</sub>) also has a vertical profile. It is unclear how these vertical distributions are taken into account? If they are neglected, which seems to be the case, the authors should estimate the error associated with these assumptions.**

*Since the NO-NO<sub>2</sub>-O<sub>3</sub> photochemical equilibrium could not be handled by the LASAT “chemical” algorithm, we decided to use measured data (O<sub>3</sub> mixing ratio, NO<sub>2</sub> photolysis rate, s. sect. 2.2.2) to convert the calculated 3D-NO mixing ratio to the photo-stationary 3D-NO<sub>2</sub> mixing ratio. As far as the distribution of O<sub>3</sub> mixing ratio within the boundary layer is concerned: a constant vertical O<sub>3</sub> mixing ratio (up to 1500 m a.gr.) is assumed over Milan oasis. This is justified by the fact, that particularly in arid and hyper-arid landscapes at mid-day conditions (maximum of insolation) the entire atmospheric boundary layer is intensively mixed, which is due to extensive convective heating of the surface by the sun which produces buoyant thermals that establish the so-called mixing layer. Consequently a uniform vertical mixing ratios is expected for trace gases without distinct local sources and lifetimes greater than exchanges times within the Boundary Layer. (c.f. Husar et al. 1978, Stull 1988). This assumption is valid for ozone. Vertically constant O<sub>3</sub> mixing ratio has been reported for the atmospheric boundary layer over semi-arid southern Africa (Meixner et al., 1993). As far as the vertical profile of j(NO<sub>2</sub>) is concerned: basically, the downward component of the actinic flux increases with increasing elevation due to the decreasing optical thickness of the scattering air masses. However, the altitude effect on the actinic flux in the first kilometer of the troposphere is typically very small. Trebs et al. (2009) used the Tropospheric Ultraviolet Visible model (TUV, version 4.4; <http://cprm.acd.ucar.edu/Models/TUV/>) to calculate the typical vertical change of the actinic flux and found a vertical gradient of 1.1%/km. Consequently, our calculations of the NO to NO<sub>2</sub> conversion in*

the boundary-layer over Milan oasis (1500 m a.gr.) have not considered any potential vertical change of the  $j(\text{NO}_2)$  values measured at ground level.

**P19372, L5: More attention should be paid at the local time at which measurements and model simulations have taken place. For instance, in Figure 4, it is unclear what the local time was for the MAX-DOAS measurements shown. This is important, in view of the diurnal cycle in soil  $\text{NO}_x$  emissions (presumably higher at mid-day in response to higher soil temperatures) and the diurnal cycle in  $\text{NO}_2$  concentrations with a midday minimum in  $\text{NO}_2$  reflecting higher mid-day OH-levels (e.g. Fig. 7).**

The authors like to thank referee#2 for this comment. As far as Fig. 4 (in MS: Fig 5) is concerned, the MAX-DOAS measurements were performed between 6:00 and 19:00 (local time) and all the “labelling” of data points are in terms of the measurements time.

**P19372, L5: The community would benefit from an evaluation of Eq. 10 with the laboratory net-derived potential net  $\text{NO}$ -fluxes. To my knowledge, such an evaluation with samples from the field has not yet been done.**

Based on this important suggestion of referee#2 we evaluated the laboratory net-derived potential net  $\text{NO}$ -fluxes according to eq. (10). In the revised version of our manuscript one will find the following figure:

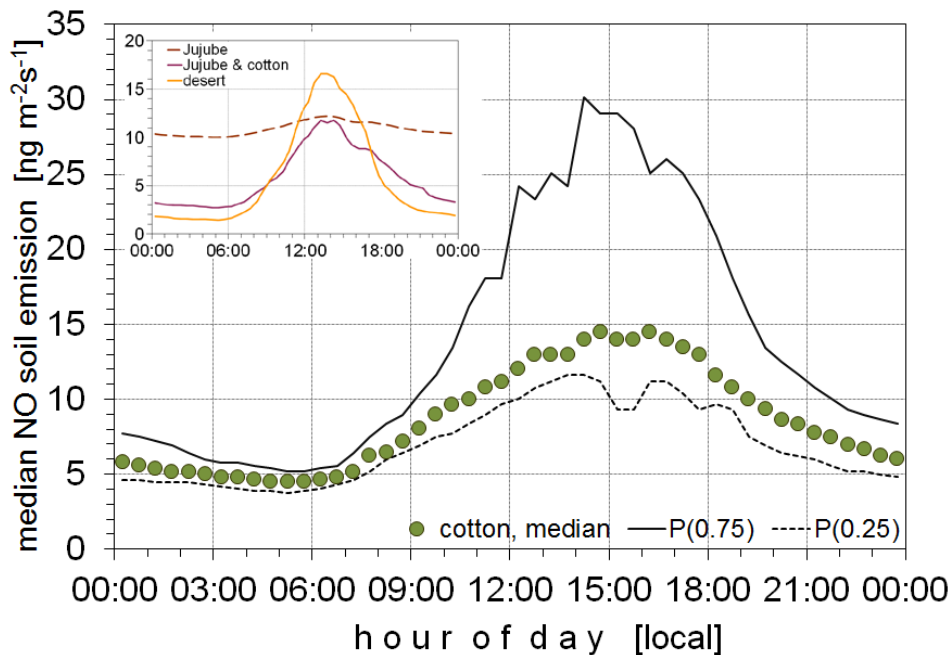


**Figure 4:** median diel variation of the actual  $\text{NO}$ -flux ( $\text{ng m}^{-2}\text{s}^{-1}$ ; in terms of mass of nitric oxide) from soils of the four major land-cover types of Milan oasis for the period 03 to 24 June, 2011. Data have been calculated according eq.(10) using (a) soil temperatures (medians) measured for each of the four major land-cover types, and (b) so-called “wilting point”-data for corresponding soil moisture contents at the four sites (s. section 2.2.3). Data for the cotton-site are given as medians, as well as 25 and 75% quantiles, those for the Jujube, Jujube-cotton and desert sites as medians only (s. figure insert).

Within the revised version of our manuscript, the following text will replace lines 1-9 on page 19377 (section 3.2):

For the period 03 to 24 June, 2011, land-cover specific, actual NO fluxes were calculated according to eq.(10) for cotton, jujube, cotton/jujube, and desert soils from corresponding laboratory derived net potential NO fluxes. As input we used land-type specific, measured soil temperature data as well as land-type specific soil moisture data (so-called “wilting points”, s. Sect. 2.2.3). The calculated NO fluxes are shown as median diel variation in Fig. 4. Since NO fluxes from Milan cotton fields dominate the total soil biogenic NO emission of the oasis, corresponding medians and quartiles are shown in Fig. 4, while – for the sake of clarity –for jujube, cotton/jujube, and desert only medians are given. Since land-type specific “wilting points” are constant, diel variations of actual NO fluxes mirror directly those of corresponding soil temperatures, showing the daily minimum around 06:00 local time for all four major land-cover types. The maximum of the actual NO-flux, however, is around 13:00 local time for jujube, cotton/jujube, and desert soils, and 15:00 local time for cotton. This is due to the increasing growth of the cotton plants, where at the beginning of the experimental period the bare soil surface was nearly 100% exposed to insolation, while towards the end of the experimental period the growing cotton canopy has shaded great parts of the soil surface. This is also reflected by the skewed distribution of actual NO-fluxes from cotton covered soil, indicated by the daytime non-symmetric inter-quartile range (upper quartile >> lower quartile). Actual NO-flux data of 09 June, 2011 (08:30-14:30 local time) were used for the comparison of LASAT and MAX-DOAS results. During this particular day (within the first week of the experimental period), the derived flux for “land-cover cotton” ranged from 15–64  $\text{ng m}^{-2}\text{s}^{-1}$  (in terms of mass of NO), those for jujube, cotton/jujube, and desert land-covers ranged from 11–13, 6–16, and 6–17  $\text{ng m}^{-2}\text{s}^{-1}$ , respectively. These actual NO fluxes were then assigned to each individual source unit (i.e. to each of the 2500 polygons of Milan oasis’ domain). The soil biogenic NO emission from all cotton fields between 08:30 and 14:30 was estimated to 28.7 kg (in terms of mass of NO), equivalent to 76% of the total soil biogenic NO emission of the entire Milan oasis.

**P19372, L5:** Also, the paper would improve greatly if the authors could indicate whether their evaluation of the LASAT simulations with the MAX-DOAS observations is consistent with the parametrization of the diurnal cycle in soil NO<sub>x</sub> emissions that follows Eq. (10).

Referee#2 is most likely pointing to the fact, that the actual NO emissions (irrespective of the land-cover type) have their maximum in the early afternoon (s. above), while the highest height-integrated NO<sub>2</sub> concentrations as simulated by LASAT (on the basis of the actual NO emissions) are in the morning (08:30–10:00), followed by rather constant values for the remainder of the day (s. Fig. 7, in MS Fig. 8). The apparent discrepancy between both diurnal variations can be simply explained by the diurnal variation of the wind direction and the specific viewing geometry of the MAX-DOAS instrument. The MAX-DOAS instrument was located at the south-west corner of the oasis, and the observations at zenith and low elevation angles probed air masses located at different locations across the oasis. The wind direction was from north-east in the morning and turned to north-west in the afternoon. Hence, air masses of lower concentration crossed the viewing directions in the afternoon compared to those in the morning. This explains that in spite of the larger NO<sub>x</sub> emissions smaller column densities have been observed in the afternoon. The apparent discrepancy of the diurnal cycles of NO emissions and measured NO<sub>2</sub> column densities indicates the importance to exactly consider the 3-dimensional NO<sub>2</sub> distribution (due to the soil-emitted NO) for the comparison of the model results with MAX-DOAS observations. We added this information to the text

**P19379, L7:** In section 3.5, the authors state that ‘there is remarkable good agreement’ between measured and simulated data. Inspection of Figure 7 however shows that there is a discrepancy of 25-30% between the LASAT model and most reliable MAX-DOAS measurement (at 15 deg elevation), with LASAT being too high. While I agree that the authors have done an impressive job in describing the spatial and temporal detail of soil

**NO<sub>x</sub> emissions from the area, I think it is a bridge too far to claim that the agreement between simulated and measured NO<sub>2</sub> is remarkable. I think the discrepancy needs more attention. It could be caused by the lack of chemistry in the LASAT simulation (NO<sub>2</sub> too long-lived).**

*Nevertheless, for the case of our measurements the locally enhanced NO values caused by the soil emissions have a small but systematic effect on the ozone concentration, and thus also on the Leighton ratio: Close to the surface (below about 50m) the NO concentrations can be quite large, with maximum values up to about 10 ppb. Consequently, the ozone concentration will be reduced due to the reaction with NO by up to about 10 ppb. This means that the Leighton ratio will be reduced by up to about 25%. Although the reduction of the ozone mixing ratio will be partly compensated by mixing with air from higher altitudes, the simulated NO<sub>2</sub> mixing ratios might overestimate the true NO<sub>2</sub> mixing ratios by up to about 25%. Probably the true overestimation for our measurements is much smaller because the typical NO mixing ratio within the lowest 100m is much lower than 10 ppb. However, the LASAT simulation overestimate slightly the true NO<sub>2</sub> VCD. The both measured and simulated NO<sub>2</sub> VSDs in Figure 7 (in MS Version Figure 8) have with an average root mean square (RMS) error between the measured and simulated values of approx. 5-15%. The overestimation of LASAT simulation is well suited to the fact that in reality a little less NO can be converted to the NO<sub>2</sub> because of lower ozone concentration at the surface. We added this information to the text.*

**It is also intriguing that the 2 and 4 deg elevation cases (for which the geometrical AMF will lead to errors) show better agreement than the 15 deg elevation case (for which the simple geometrical AMF works fine). These aspects should be discussed in more detail than just claiming 'remarkable agreement'.**

*The reviewer is right that in principle the accuracy of the geometric approximation is much higher for the high elevation angles than for the lower elevation angles. However, for the specific cases studied here, this is not the case. First, close to the sources, the height of the layer with elevated NO<sub>2</sub> is quite low (in our case the bulk of NO<sub>2</sub> is located below 50 m). Secondly, also the aerosol load is usually very low at Milan oasis. Thus the probability of scattering events inside the layer of enhanced NO<sub>2</sub> is very low, and consequently the accuracy of the geometric approximation is relatively high. To further quantify the associated uncertainties, we performed radiative transfer simulations and found that the deviations of the geometric approximation are similar for the different elevation angles (about 5% for 2°, 3% for 4° and 3% for 15°).*

*However, because of the shorter light paths through the NO<sub>2</sub> layer, the relative error caused by the uncertainty of the spectral analysis is higher than for the low elevation angles. Thus for the case of our measurements, we indeed expect lower uncertainties for the low elevation angles. We added this information to the text.*

#### **Specific comments:**

**1. P19362, L25-26: I'm not sure if the assumption that free tropospheric NO<sub>2</sub> advection is negligible holds. In the study-area, considerable contributions from lightning and soil (from other areas) resulting in summertime NO<sub>2</sub> maxima have been reported (e.g. van der A et al., 2008; Miyazaki et al., ACP, 2012 – Figure 14).**

- *We agree that in principle tropospheric NO<sub>2</sub> retrievals might be also affected by NO<sub>x</sub> produced from lightning. Very fortunately, the study area is typically only little affected by clouds and aerosols. Also the lightning activity is rather weak. The selected study area provides rather good pre-requisites to achieve this aim of the study, since they are supposed not to be strongly affected by other, neighboring substantial NO<sub>x</sub> sources, such as e.g. traffic or power plants; also NO<sub>x</sub> emissions due to lightning can be neglected over Milan oasis. It should also be noted that*

*lightning (and soil emissions from other areas) would affect both the upwind and downwind areas in the same way.*

**2. P19363, L8: here 'NE' is mentioned, but in L11 'NW' is mentioned. Should it be NW everywhere? Please clarify if NW means 'North West'.**

- *The authors like to thank Anonymous Referee #2 for his/her comment concerning our typing mistake. There was a simple typo ("NW" instead of "NE")*

**3. P19363, L19: please have the list of references preceded by e.g.**

*"e.g." have been added in the revised MS.*

**4. P19365, L5-6: Strongly suggest to provide references that confirm that scattering may be neglected at elevation angles > 15 degrees.**

- *The potential importance of scattering on the interpretation of the MAX-DOAS measurements depends on two main aspects: first on the height of the trace gas layer. Second on the amount of aerosols. In our case the trace gas layer is shallow and the aerosol amount is low. Thus scattering effects can be neglected. (see discussion of last major point above).*

**5. P19365, L8: I don't think the abbreviation or meaning of LASAT has been introduced at this stage. Suggest to do so.**

- *In abstract the abbreviation of LASAT (Lagrangian Simulation of Aerosol-Transport) was explained. However, here "Lagrangian Simulation of Aerosol-Transport " has been added.*

**6. P19367, L4: the section title should read 'NO fluxes', not 'NO<sub>2</sub> fluxes'.**

- *Many thanks to Anonymous Referee #2 for his/her comment concerning our typing mistake. There was a typo ("NO<sub>2</sub>" instead of "NO")*

**7. P19368, L7: please clarify why the soil T variation between 20 and 30 degrees is 'desired'. Do ambient temperatures in July never drop below 20 C?**

- *The control of the soil temperature via the temperature controlled cabinet of the soil laboratory must allow the frequent (and fast) change at least between two temperatures differing by 10 K ( $T_0$  and  $T_1$ ) during an individual drying-out experiment (please see Behrendt et al. 2014). Normally, the ambient temperatures in July of the study area are above 20 °C. We added the reference to the text.*

**8. P19368, L17: after 'As shown during the last two decades', a few citations would be appropriate.**

- *„Yang and Meixner, 1997; Otter et al., 1999; Kirkman et al., 2001; van Dijk and Meixner, 2001; van Dijk et al., 2002; Garrido et al., 2002; Meixner and Yang, 2006; Yu et al., 2008, 2010; Feig et al., 2008; Ashuri, 2009; Feig, 2009; Laville et al., 2009; Gelfand et al., 2009; Bargsten et al., 2010“ have been added.*

**9. P19371, L2: 'methods' should be 'method'.**

- *"methods" has been corrected for "method" in revised MS.*

**10. P19371, L5: the closing bracket after plant cover is redundant.**

- *"the closing bracket" was removed.*

**11. P19372, L23: in terms of stability classes.**

- *"of" has been added.*

**12. P19377, L9: 76% of total, 24-hour soil biogenic NO emissions? Please clarify.**

- *That is not 76% of 24-hour soil biogenic NO emissions, but also 75% of the total soil NO emission between 08:30 and 14:30. Here additional "within 6 hours" has been added.*

**13. P19378, L14-16: the resolution of Figure 6 is a bit low. I think the Figure is so nice that it would merit an improvement in resolution so the spatial detail can be better distinguished.**

- *We followed the suggestions of Anonymous Referee #2.*

Stull, R.B. (1988), *An Introduction to Boundary-Layer Meteorology*, Kluwer Academic Publishers, Dordrecht, The Netherlands.

Husar, R.B., Patterson, D.E., Husar, J.D., Gillani, N.V., Wilson Jr., W.E. (1978), Sulfur budget of a power plant plume, *Atmospheric Environment*, 12 (1-3), 549-568.

Meixner, F.X., Ajavon, A.-L., Helas, G., Scharffe, D., Zenker, T., Harris, G.W., Andreae, M.O. (1993), Vertical distribution of ozone over southern Africa: Airborne measurements during SAFARI-92, AGU Fall Meeting, San Francisco, U.S.A.

Trebs, I., Bohn, B., Ammann, C., Rummel, U., Blumthaler, M., Königstedt, R., Meixner, F. X., Fan, S., Andreae, M.O. (2009), Relationship between the NO<sub>2</sub> photolysis frequency and the solar global irradiance, *Atmospheric Measurement Techniques*, 2, 725–739.

1 **Tropospheric vertical column densities of NO<sub>2</sub> over managed dryland ecosystems**  
2 **(Xinjiang, P. R. China): MAX-DOAS measurements vs. 3-D dispersion model**  
3 **simulations based on laboratory derived NO emission from soil samples**

4

5 Buhalgem Mamtimin<sup>1\*</sup>, Thomas Behrendt<sup>1</sup>, Moawad M. Badawy<sup>1,2</sup>, Thomas Wagner<sup>3</sup>, Yue  
6 Qi<sup>1,4</sup>, Zhaopeng Wu<sup>1,5</sup> and Franz X. Meixner<sup>1</sup>

7

8 <sup>1</sup>*Biogeochemistry Department, Max Planck Institute for Chemistry, Mainz, Germany.*

9 <sup>2</sup>*Department of Geography, Faculty of Arts, Ain-Shams University, Egypt.*

10 <sup>3</sup>*Air Chemistry Department, Max Planck Institute for Chemistry, Mainz, Germany.*

11 <sup>4</sup>*International Cooperation Department, National Center for Climate Change Strategy and*  
12 *International Cooperation, Beijing, P. R. China.*

13 <sup>5</sup>*Institute of Geography Science, Xinjiang Normal University, China,*

14

15 \*Corresponding author: buhalgem.mamtimin@mpic.de

16

17

18

19

20 **Abstract**

21 We report on MAX-DOAS observations of NO<sub>2</sub> over an oasis-ecotone-desert ecosystem in  
22 NW-China. There, local ambient NO<sub>2</sub> concentrations originate from enhanced biogenic NO  
23 emission of intensively managed soils. Our target oasis “Milan” is located at the southern  
24 edge of the Taklimakan desert, very remote and well isolated from other potential anthropoge-  
25 nic and biogenic NO<sub>x</sub> sources. Four observation sites for MAX-DOAS measurements were  
26 selected, at the oasis center, downwind and upwind of the oasis, and in the desert. Biogenic  
27 NO emissions in terms of (i) soil moisture and (ii) soil temperature of Milan oasis’ (iii)  
28 different land-cover type sub-units (cotton, Jujube trees, cotton/Jujube mixture, desert) were  
29 quantified by laboratory incubation of corresponding soil samples. Net potential NO fluxes  
30 were up-scaled to oasis scale by areal distribution and classification of land-cover types  
31 derived from satellite images using GIS techniques. A Lagrangian dispersion model (LASAT,  
32 Lagrangian Simulation of Aerosol-Transport) was used to calculate the dispersion of soil  
33 emitted NO into the atmospheric boundary layer over Milan oasis. Three dimensional NO  
34 concentrations (30 m horizontal resolution) have been converted to 3-D (three dimensional)  
35 NO<sub>2</sub> concentrations, assuming photostationary state conditions. NO<sub>2</sub> column densities were  
36 simulated by suitable vertical integration of modeled 3-D NO<sub>2</sub> concentrations at those  
37 downwind and upwind locations, where the MAX-DOAS measurements were performed.  
38 Downwind-upwind differences (a direct measure of Milan oasis’ contribution to the areal  
39 increase of ambient NO<sub>2</sub> concentration) of measured and simulated slant (as well as vertical)  
40 NO<sub>2</sub> column densities show excellent agreement. This agreement is considered as the first  
41 successful attempt to prove the validity of the chosen approach to up-scale laboratory derived  
42 biogenic NO fluxes to ecosystem field conditions, i.e. from the spatial scale of a soil sample  
43 (cm<sup>2</sup>) to the size of an entire agricultural ecosystem (km<sup>2</sup>).

44

45 **1 Introduction**

46 Emissions of nitric oxide (NO) are important in regulating chemical processes of the atmo-  
47 sphere (Crutzen, 1987). Once emitted into the atmosphere, NO reacts rapidly with ozone (O<sub>3</sub>)  
48 to nitrogen dioxide (NO<sub>2</sub>) which, under daylight conditions, is photolyzed back to NO ( $\lambda \leq$   
49 420 nm). For that reason, NO and NO<sub>2</sub> are usually considered as NO<sub>x</sub> (NO<sub>x</sub> = NO + NO<sub>2</sub>).  
50 Ambient NO<sub>x</sub> is a key catalyst in atmospheric chemistry: during the atmospheric oxidation of  
51 hydrocarbons its ambient concentration determines whether ozone (O<sub>3</sub>) is photochemically  
52 generated or destroyed in the troposphere (Chameides et al., 1992). While the combustion of  
53 fossil fuels (power plants, vehicles) is still the most important global NO<sub>x</sub> source (approx. 25  
54 Tg a<sup>-1</sup> in terms of mass of N), biogenic NO emissions from soils have been estimated to range  
55 between 6.6 and 9.6 Tg a<sup>-1</sup> (Denman et al., 2007). The considerable uncertainty about the  
56 range of soil biogenic NO emissions stems from widely differing estimates of the NO  
57 emission. Moreover, the uncertainties in the NO emission data from semi-arid, arid, and  
58 hyper-arid regions are very large (mainly due to a very small number of measurements being  
59 available). These ecosystems, however, are considered to contribute more than half to the  
60 global soil NO source (Davidson and Kinglerlee, 1997), and make approx. 40% of planet  
61 Earth's total land surface (Harrison and Pearce, 2000).  
62 Production (and consumption) of NO in the soil depends mainly on soil microbial activity and  
63 is mainly controlled by soil temperature, soil moisture, and soil nutrient concentration  
64 (Conrad, 1996; Meixner and Yang 2006; Ludwig et al., 2001). Any natural or anthropogenic  
65 action that result in the inputs of nutrients (e.g. by fertilizer application) and/or modification  
66 of soil nutrient turnover rates has a substantial effect on soil biogenic NO emission. The rapid  
67 (economically driven) intensification of arid agriculture (oasis agriculture), particularly by en-  
68 largement of the arable area and by enhancement of necessary irrigation leads inevitably to  
69 the increase of soil biogenic NO emissions. Since those microbial processes which underlay  
70 NO production and NO consumption in soils are confined to the uppermost soil layers  
71 (<0.05 m depth, Rudolph et al., 1996), the most direct method for their characterization and  
72 quantification is usually realized by laboratory incubation of soil samples; corresponding  
73 measurements result in the determination of so-called net potential NO fluxes, which are  
74 explicit functions of soil moisture, soil temperature, and ambient NO concentration (Behrendt  
75 et al., 2014).  
76 Tropospheric NO<sub>2</sub> column densities can be retrieved from satellite observations using  
77 differential optical absorption spectroscopy (DOAS) (e.g. Leue et al., 2001; Richter and  
78 Burrows, 2002, Beirle et al., 2004). Identification and quantification of the sources of

79 tropospheric NO<sub>2</sub> column densities are important for monitoring air quality, for understanding  
80 radiative forcing and its impact on local climate. Ground-based Multi Axis Differential  
81 Optical Absorption Spectroscopy (MAX-DOAS) is a novel measurement technique  
82 (Hönninger et al., 2004) that represents a significant advantage over the well-established  
83 zenith scattered sunlight DOAS instruments, which are mainly sensitive to stratospheric  
84 absorbers. From NO<sub>2</sub> slant column densities, retrieved from measurements at different  
85 elevation angles, information about tropospheric NO<sub>2</sub> profiles and/or tropospheric vertical  
86 column densities can be obtained (e.g. Sinreich et al., 2005; Wittrock et al., 2004; Wagner et  
87 al., 2011).

88 In this paper we concentrate (a) on ground-based MAX-DOAS measurements of slant and  
89 vertical NO<sub>2</sub> column densities over an intensively used oasis of the Taklimakan desert (NW-  
90 China), (b) on biogenic NO emissions derived from laboratory incubation measurements on  
91 oasis soil samples, (c) on up-scaling of the laboratory results to the oasis level, (d) calculation  
92 of atmospheric boundary layer NO<sub>2</sub> concentrations by suitable NO→NO<sub>2</sub> conversion and  
93 3 dimensional dispersion modelling, and (e) on simulating slant and vertical NO<sub>2</sub> column den-  
94 sities from the calculated 3-D-NO<sub>2</sub> distributions by integration along the MAX-DOAS light  
95 path. The final aim is comparison and discussion of the results obtained under (a) and (e).

96

## 97 **2 Materials and methods**

### 98 **2.1 Research area**

99 After two ‘searching field campaigns’ (2008 and 2009) in the Xinjiang Uighur Autonomous  
100 Region of NW-China, the oasis “Milan” has been identified as the target oasis for the  
101 presented research. The contemporary oasis Milan, identical to the ancient silk-road post  
102 “Miran”, belongs to the county “Ruoqiang” of the Xinjiang province and is located in the  
103 southern Taklimakan Desert on the foot of the Altun Shan Mountains (39.25 °N, 88.92 °E,  
104 998 m a.s.l.). In the early 1950s, the delta-shaped oasis (see Fig. 1) has been established as an  
105 agricultural co-operative “state farm” (*Xinjiang Production and Construction Crop*) and  
106 covers nowadays about 100 km<sup>2</sup>. Milan oasis can be geomorphologically classified as a  
107 “mountain-oasis-ecotone-desert system (MOED system)” consisting of Gobi (gravel) desert, a  
108 salty transition zone surrounding the oasis, and dryland farming with irrigation. The latter  
109 consists only of two crops, cotton and jujube trees (*Ziziphus Jujuba* L., “red date”), which are  
110 planted, irrigated, and fertilized following standardized protocols and growing on rectangular  
111 fields (approx. 10 ha) of pure cultures or mixtures of it. The general energy supply of Milan

112 oasis is entirely provided by nearby hydropower plants, and battery powered trikes dominate  
113 the local public and private transport. Consequently, anthropogenic NO<sub>x</sub> emissions of Milan  
114 oasis are considered as very low, if not negligible. Beyond that, Milan oasis is isolated by the  
115 desert from neighbouring oases by 80 to 400 km. Therefore, the dominant NO<sub>x</sub> source of Mi-  
116 lan oasis are biogenic NO emissions from its intensively managed crop fields; the oasis can be  
117 undoubtedly considered as a large "hotspot in the middle of nothing". Given this very specific  
118 situation, it is certainly justified to assume that (a) NO<sub>2</sub> concentrations in the atmospheric  
119 boundary layer over Milan oasis are only caused by the oasis itself, and (b) free tropospheric  
120 NO<sub>2</sub> concentrations, which are usually due to large-scale tropospheric NO<sub>2</sub> advection, are  
121 negligible.

122 | According to Koeppen classification ([Koeppen, 1931](#); [Kottek et al., 2006](#)), Milan oasis owns  
123 a cold desert climate (BWk), which is dominated by long hot summers (30 years' mean:  
124 29°C) and cold winters (30 years' mean: -6°C). Mean annual precipitation amounts  
125 28.5 mm, mean annual evaporating capacity is 2920 mm, mean wind direction is NE to E, and  
126 | mean wind speed is 2.7 m s<sup>-1</sup>.

## 127 **2.2 *In-situ* measurements**

128 A field campaign has been performed at Milan oasis, from 24 May to 26 June, 2011. A total  
129 of 32 individual MAX-DOAS measurements (approx. 20 min) have been performed by two  
130 Mini-MAX-DOAS instruments (partially simultaneously) on 21 days during the 2011 cam-  
131 paign at the NE natural forest site (1), desert site (2), jujube site (3) and hotel station in Milan  
132 oasis center (4). Accompanying data of wind direction, wind speed, air temperature,  
133 barometric pressure, global and net radiation have been observed at sites (1) – (5) at 1.8 m  
134 | above ground (at [NE](#) natural forest: 11 m; at hotel station: 23 m). Soil temperature (at 0.05 m  
135 depth), as well as rainfall (amount and intensity) were recorded at all sites in 2011.

### 136 **2.2.1 Ground-based measurements of vertical column densities of NO<sub>2</sub>**

137 Multi-Axis-Differential Optical Absorption Spectroscopy (MAX-DOAS) observes scattered  
138 sun light under various (mostly slant) elevation angles. From combinations of the retrieved  
139 NO<sub>2</sub> slant column densities (SCDs) obtained at different elevation angles, information on the  
140 vertical NO<sub>2</sub> profile and/or on the corresponding vertical column density (VCD) can be  
141 | obtained ([e.g.](#) [Hönninger et al., 2002](#); [Sinreich et al., 2005](#); [Wittrock et al., 2004](#); [Wagner et](#)  
142 [al., 2011](#)). Spectral calibration of the MAX-DOAS instruments was performed by fitting a  
143 measured spectrum to a convoluted solar spectrum based on a high resolution solar spectrum

144 (Kurucz et al., 1984). Several trace gas absorption cross sections of NO<sub>2</sub> at 294 K (Vandaele  
 145 et al., 1996), H<sub>2</sub>O at 290 K (Rothman et al., 2005), Glyoxal at 296 K (Volkamer et al., 2005),  
 146 O<sub>3</sub> at 243 K (Bogumil et al., 2003) and O<sub>4</sub> at 286K (Hermans et al., 1999) were convolved to  
 147 match the resolution of the instrument and then used in the spectral analysis using a  
 148 wavelength range of 420-450 nm (also a Ring spectrum was included in the fitting process).  
 149 The output of the spectral analysis is the NO<sub>2</sub> SCD, which represents the NO<sub>2</sub> concentration  
 150 integrated along the corresponding light paths through the atmosphere.  
 151 Since a spectrum measured in zenith direction (a so called Fraunhofer reference spectrum) is  
 152 included in the fit process to remove the strong Fraunhofer lines, the retrieved NO<sub>2</sub> SCD ac-  
 153 tually represents the difference between the SCDs of the measurement and the Fraunhofer  
 154 reference spectrum; it is usually referred to as differential SCD or DSCD<sub>meas</sub>. The troposphe-  
 155 ric DSCD for the elevation angle  $\alpha$  can be derived from MAX-DOAS observation by subtract-  
 156 ing the NO<sub>2</sub> DSCD for the closest zenith observation ( $\alpha_0 = 90^\circ$ ):

$$157 \quad DSCD_{trop}(\alpha) = DSCD_{meas}(\alpha) - DSCD_{meas}(\alpha_0) \quad (1)$$

158 DSCDs are converted into VCDs (the vertically integrated concentration) using so called air  
 159 mass factors (AMF, Solomon et al., 1987), which is defined by:

$$160 \quad AMF = SCD / VCD \quad (2)$$

161  
 162 In many cases AMF are determined from radiative transfer simulations (Solomon et al.,  
 163 1987). However, if trace gas column densities are retrieved from MAX-DOAS observations at  
 164 high elevation angles ( $> 10^\circ$ ), the AMF can be determined by the so called geometric approxi-  
 165 mation (Hönninger et al., 2002; Brinkma et al., 2008; Wagner et al., 2010):

$$166 \quad AMF_{trop} \approx \frac{1}{\sin(\alpha)} \quad (3)$$

167  
 168 In this study, the tropospheric vertical column density (VCD<sub>trop</sub>) is obtained from DSCD<sub>trop</sub>( $\alpha$ )  
 169 as discussed by Wagner et al. (2010):

$$170 \quad VCD_{trop} = \frac{DSCD_{trop}(\alpha)}{AMF_{trop}(\alpha) - AMF_{trop}(\alpha_0)} \quad (4)$$

171 During the field experiments, the MAX-DOAS instruments have been mounted on solid  
 172 tables (aluminium structure) at approx. 11 m a.gr. (NW natural forest, hotel station) and 3.5 m

173 a.gr. (remainder of sites) with the telescope facing northwards. Observations were always  
174 made on elevation angles of 0°, 2°, 4°, 6°, 8°, 10°, 15°, 20°, 45° and 90°.  $VCD_{tropS}$  were  
175 determined from measurements at 15°. The potential importance of scattering on the  
176 interpretation of the MAX-DOAS measurements depends on two main aspects: first on the  
177 height of the trace gas layer and second on the amount of aerosols. In our case the trace gas  
178 layer is shallow and the aerosol amount is low (see 2.2.8). Thus scattering effects can be  
179 neglected. However, for comparison of the  $DSCD_{trop}$  data obtained by MAX-DOAS with the  
180 simulated SCDs obtained from 3 D distributions of  $NO_2$  concentration (calculated with  
181 LASAT (Lagrangian Simulation of Aerosol-Transport)) on the basis of laboratory derived net  
182 potential  $NO_2$  fluxes) the lower elevation angles (2°, 4°) for  $DSCD_{trop}(\alpha)$  have been used,  
183 which have a much higher sensitivity to the observed  $NO_2$ .  
184 For classifying all MAX-DOAS measurements whether they were made up-wind, down-wind,  
185 or in the center of Milan oasis, their observation position was related to the mean wind  
186 direction during each measurement period. Wind measurements were part of accompanying  
187 *in-situ* measurements (see below).

### 188 **2.2.2 Accompanying measurements**

189 Wind direction, wind speed, air temperature, relative humidity, barometric pressure, and  
190 rainfall intensity have been measured by combined weather sensors (weather transmitter  
191 WXT510, Vaisala, Finland). All five weather sensors have been operated side-by-side for one  
192 week before they have been mounted at the individual measurement sites (1) – (5). Based on  
193 these results, all meteorological data, which have been measured between 3 – 24 July, 2011  
194 have been corrected using one of the sensors as reference. All combined weather sensors'  
195 data, as well as those of net radiation (4 component net radiation sensor, model NR01,  
196 Hukseflux, The Netherlands) and soil temperature (thermistor probe, model 109, Campbell  
197 Scientific, U.S.A.) have been recorded every minute. Ambient  $O_3$  concentrations and  $NO_2$   
198 photolysis rates have also been measured in-situ; both quantities are necessary to calculate the  
199  $NO \rightarrow NO_2$  conversion factor (see Sect. 2.2.8). Ozone concentrations have been measured by  
200 UV-absorption spectroscopy (model 49i, ThermoFisher Scientific, U.S.A.) and  $NO_2$  photoly-  
201 sis rate by a filter radiometer (model 2-Pi-JNO<sub>2</sub>, metcon, Germany) in 1 minute intervals.

### 202 **2.2.3 Soil samples**

203 Microbial processes responsible for biogenic NO emission are confined to the uppermost soil  
204 layers (Galbally and Johansson, 1989; Rudolph et al., 1996; Rudolph and Conrad, 1996).

205 Consequently, composite soil samples (1 kg of top soil, 0–5 cm depth) have been collected at  
206 the individual sites of Milan oasis (natural forest, cotton, jujube, cotton & jujube mixture,  
207 desert). All samples (air dried) were sent from Xinjiang to Germany by air cargo and stored  
208 refrigerated (+ 4°C) until laboratory analysis of the net potential NO flux (see below). Sub-  
209 samples have been analyzed for dry bulk soil density (ISO 11272), pH (ISO 10390), electrical  
210 conductivity (salinity, ISO 11265), contents of nitrate and ammonium (ISO 14256), total  
211 carbon and total nitrogen (ISO 10649 and ISO 13878), texture (ISO 11277), as well of soil  
212 water potential (pF values 1.8, 2.5, 4.2, Hartge and Horn, 2009).  
213 Electrical conductivity varied between 1.6 to 9.5 dS m<sup>-1</sup> within the managed soils, and was  
214 59.8 and 3.0 dS m<sup>-1</sup> in the natural forest and desert soils, respectively. Commercially available  
215 soil moisture probes (e.g. TDR ([Time-Domain-Reflectometry](#)) and FDR ([Frequence-Domain-](#)  
216 [Reflectometry](#))) show extreme interferences for soils of >2 dS m<sup>-1</sup> (c.f. Kargas et al., 2013)  
217 and their calibration for such soils is extremely challenging, if possible at all. Indeed, FDR-  
218 signals monitored in Milan oasis' soils were extremely noisy and spurious. Nevertheless, up-  
219 scaling of the laboratory derived net potential NO fluxes needs data of the uppermost layer of  
220 each soil of Milan oasis land-types (see Sect. 2.2.6). For that, as most reasonable  
221 approximation, it was decided to use that individual (constant) gravimetric soil moisture  
222 content, which corresponds to the so-called “wilting point”. The latter was determined by  
223 laboratory water tension measurements (pF 4.2) on undisturbed soil cores from each land-  
224 cover type. The wilting point is defined as that soil moisture in the root zone, which would  
225 cause irreversible wilting of plants. Wilting point conditions in the uppermost soil layers  
226 (2 cm) of soils in the Taklimakan Desert are easily reached, since evaporation ~~there is~~  
227 extremely high (evaporating capacity 2920 mm a<sup>-1</sup>). Even after flooding irrigation of Milan  
228 oasis' crop fields, these conditions have repeatedly been observed within at least 3 days by  
229 visual inspections.

#### 230 **2.2.4 Laboratory determination of net potential NO<sub>2</sub> fluxes**

231 The methodology for the laboratory measurement of the NO flux from soil has been deve-  
232 loped at the end of the nineties (Yang and Meixner, 1997) and has been continuously used  
233 during the last two decades (Otter et al., 1999; Kirkman et al., 2001; van Dijk and Meixner,  
234 2001; Feig et al., 2008a; Feig et al., 2008b; Yu et al., 2008; Ashuri, 2009; Feig, 2009; Gelfand  
235 et al., 2009; Yu et al., 2010a, 2010b; Bargsten et al., 2010). The methodology has been  
236 significantly improved in the frame of this study and is described in detail by Behrendt et al.  
237 (2014).

238 Generally, the release of gaseous NO from soil is the result of microbial NO production and  
239 simultaneous NO consumption. The latter is, as shown by Behrendt et al. (2014), particularly  
240 for arid and hyper-arid soils, negligible. Applying the laboratory dynamic chamber method,  
241 the release of NO is determined by incubating aliquots of the soil samples in a dynamic  
242 chamber system under varying, but prescribed conditions of soil moisture, soil temperature,  
243 and chamber's headspace NO concentrations. From the difference of measured NO concentra-  
244 tions at the outlets of each soil containing chamber and an empty reference chamber, actual  
245 net potential NO fluxes (in terms of mass of nitric oxide per area and time) is calculated as  
246 function of soil moisture and soil temperature. For that, a known mass (approx. 60 g dry  
247 weight) of sieved (2 mm) and wetted (to water holding capacity) soil is placed in one of six  
248 Plexiglas chambers (volume  $9.7 \times 10^{-4} \text{ m}^3$ ) in a thermo-controlled cabinet (0 – 40°C). After  
249 passing through a purification system (PAG 003, Ecophysics, Switzerland), dry pressurized,  
250 zero (i.e., "NO free") air is supplied to each chamber, controlled by a mass flow controller  
251 ( $4.167 \times 10^{-5} \text{ m}^3 \text{ s}^{-1}$ ). The outlet of each chamber is connected via a switching valve system to  
252 the gas-phase chemiluminescence NO analyzer (model 42i-TL, Thermo Fisher Scientific Inc.,  
253 U.S.A.) and to the non dispersive infrared analyzer CO<sub>2</sub>/H<sub>2</sub>O-analyzer (model LI-COR 840A,  
254 LI-COR Biosciences Inc., U.S.A.). During a period of 24 – 48 h, the soil samples are slowly  
255 drying out, hence providing the desired variation over the entire range of soil moisture (i.e.  
256 from water holding capacity to wilting point conditions and completely dry soil). During the  
257 drying out period, the temperature of thermo-controlled cabinet is repeatedly changed from 20  
258 to 30°C, hence providing the desired soil temperature variation (Behrendt et al. 2014). Occa-  
259 sionally, nitric oxide standard gas (200 ppm) is diluted into the air purification system via a  
260 mass flow controller; this allows the control of the chamber headspace NO concentration  
261 when determining NO consumption rate of the soil sample. The actual soil moisture content  
262 of each soil sample is determined by considering the H<sub>2</sub>O mass balance of each chamber,  
263 where the temporal change of the chamber's headspace H<sub>2</sub>O concentration is explicitly related  
264 to the evaporation rate of the soil sample. Tracking the chamber's headspace H<sub>2</sub>O concen-  
265 tration throughout the drying-out period and relating it to the gravimetrically determined total  
266 soil mass at the start and end of the measurement period delivers the actual gravimetric soil  
267 moisture content of the soil sample (Behrendt et al., 2014).

268 As shown during the last two decades (Yang and Meixner, 1997; Otter et al., 1999; Kirkman  
269 et al., 2001; van Dijk and Meixner, 2001; van Dijk et al., 2002; Meixner and Yang, 2006; Yu  
270 et al., 2008, 2010; Feig et al., 2008; Ashuri, 2009; Feig, 2009; Gelfand et al., 2009 and  
271 Bargsten et al., 2010), the dependence of NO release from gravimetric soil moisture and soil

272 temperature can be characterized by two explicit dimensionless functions, the so-called opti-  
 273 mum soil moisture curve  $g(\theta_g)$  and the exponential soil temperature curve  $h(T_{soil})$

$$274 \quad g(\theta_g) = \left( \frac{\theta_g}{\theta_{g,0}} \right)^a \exp \left[ -a \left( \frac{\theta_g}{\theta_{g,0}} - 1 \right) \right] \quad (5)$$

$$275 \quad h(T_{soil}) = \exp \left[ \frac{\ln Q_{10,NO}}{10} (T_{soil} - T_{soil,0}) \right] \quad (6)$$

276 where  $\theta_g$  is the dimensionless gravimetric soil moisture content,  $\theta_{g,0}$  the so-called optimum  
 277 gravimetric soil moisture content (i.e., where the maximum NO release has been observed),  $a$   
 278 is the soil moisture curve's shape factor (solely derived from NO release and gravimetric soil  
 279 moisture data which have been observed during the drying-out measurements, see Behrendt et  
 280 al. 2014),  $T_{soil}$  is the soil temperature (in °C),  $T_{soil,0}$  is the reference temperature (here: 20°C),  
 281 and  $Q_{10,NO}$  is the (logarithmic) slope of  $h(T_{soil})$ , defined by

$$282 \quad Q_{10,NO} = \frac{\ln F_{NO}(\theta_{g,0}, T_{soil,1}) - \ln F_{NO}(\theta_{g,0}, T_{soil,0})}{T_{soil,1} - T_{soil,0}} \quad (7)$$

283 where  $T_{soil,1}$  is a soil temperature which is 10 K different from  $T_{soil,0}$  (here: 30°C). The actual  
 284 NO fluxes  $F_{NO}$  ( $\text{ng m}^{-2} \text{s}^{-1}$ ; in terms of mass of nitric oxide) are defined by

$$285 \quad F_{NO}(\theta_{g,0}, T_{soil,0}) = \frac{Q}{A_{soil}} \left[ n_{NO, \text{cham}}(\theta_{g,0}, T_{soil,0}) - m_{NO, \text{ref}} \right] f_{C,NO} \quad (8)$$

$$286 \quad F_{NO}(\theta_{g,0}, T_{soil,1}) = \frac{Q}{A_{soil}} \left[ n_{NO, \text{cham}}(\theta_{g,0}, T_{soil,1}) - m_{NO, \text{ref}} \right] f_{C,NO} \quad (9)$$

287 where  $Q$  is the purging rate of the dynamic chambers ( $\text{m}^3 \text{s}^{-1}$ ),  $A_{soil}$  is the cross-section of the  
 288 dynamic chamber ( $\text{m}^2$ ), and  $m_{NO, \text{cham}}$  and  $m_{NO, \text{ref}}$  are the NO mixing ratios (ppb) observed un-  
 289 der conditions  $(\theta_{g,0}, T_{soil,0})$  and  $(\theta_{g,0}, T_{soil,1})$  at the outlets of each soil chamber and the reference  
 290 chamber, respectively. The conversion of NO mixing ratios to corresponding NO concentra-  
 291 tions ( $\text{ng m}^{-3}$ , in terms of mass of nitric oxide) is considered by  $f_{C,NO}$  ( $= 572.5 \text{ ng m}^{-3} \text{ ppb}^{-1}$   
 292 under STP conditions). Finally, the net potential NO flux,  $F_{NO}(\theta_g, T_{soil})$  is given by

$$293 \quad F_{NO}(\theta_g, T_{soil}) = F_{NO}(\theta_{g,0}, T_{soil,0}) g(\theta_g) h(T_{soil}) \quad (10)$$

294 This net potential NO flux is specific for each soil sample, hence for sites (1), (2), (4), and (5)  
295 of Milan oasis; the actual NO flux of the sites is calculated applying corresponding field data  
296 of gravimetric soil moisture and soil temperature. This procedure has been successfully  
297 applied for a variety of terrestrial ecosystems (e.g., Otter et al., 1999; van Dijk et al., 2002;  
298 Ganzeveld et al., 2008). For soils of the Zimbabwean Kalahari (Ludwig et al., 2001; Meixner  
299 and Yang, 2006), for a German grassland soil (Mayer et al., 2011), but also for Brazilian  
300 rainforest soils (van Dijk et al., 2002), soil biogenic NO fluxes derived from the described  
301 laboratory incubation method have been successfully verified by field measurements using  
302 both, field dynamic chamber and micrometeorological (aerodynamic gradient) techniques.

### 303 **2.2.5 Classification and actual distribution of Milan fields**

304 Image classification is likely to assemble groups of identical pixels found in remotely sensed  
305 data into classes that match the informational categories of user interest by comparing pixels  
306 to one another and to those of known identity. For the purposes of our study, land-cover  
307 classification was carried out based on two Quickbird images (0.6 m ground resolution,  
308 DigitalGlobe, <http://www.digitalglobe.com>) acquired on 09 April and 31 August 2007  
309 respectively, with the aid of a recent ETM+ Landsat image (141/033,  
310 <http://earthexplorer.usgs.gov/>) acquired on 25 April 2011 (15 and 30 m spatial resolution). A  
311 major advantage of using Quickbird images of high spatial resolution images is that such data  
312 greatly reduce the mixed-pixel problem (a “mixed pixel” consists of several land-cover  
313 classes) and provide a greater potential to extract much more detailed information on land-  
314 cover structures (e.g. field borders, buildings, roads) than medium or coarse spatial resolution  
315 data using whether on screen digitizing or image classification.

316 However, we take the advantage of resolution merge processing to increase the spatial  
317 resolution of the Landsat image from 30 to 15 meters for the bands 1-5 and 7 for better land-  
318 cover mapping and for updating the land-cover map from 2007 to 2011. Then, we defined  
319 different areas of interests (AOIs) to represent the major land-covers with the aid of in-situ  
320 GPS data collection (45 points). Next, we increased number of AOIs based on image spectral  
321 analysis method. After that supervised classification was performed using the maximum  
322 likelihood parametric rule and probabilities. This classifier uses the training data by means of  
323 estimating means and variances of the classes, which are used to estimate Bayesian  
324 probability and also consider the variability of brightness values in each class. For that, it is  
325 the most powerful classification methods when accurate training data is provided and one of  
326 the most widely used algorithms (Perumal and Bhaskaran, 2010). As a result, five major

327 ecosystems were determined: cotton, jujube, cotton/ujube mixture fields, desert, and plant  
328 cover). The cotton and the jujube fields are the most dominant types. Finally, the classified  
329 land-cover image was converted into vector format using polygon vector data type to be  
330 implemented in LASAT analysis as sources of NO flux and for the purpose of estimating NO  
331 concentrations. The map includes 2500 polygons of different sizes as sub-units of Milan  
332 major land-cover.

### 333 **2.2.6 Two dimensional distribution of soil NO emissions of Milan oasis**

334 The soil NO emission sources of Milan oasis were defined by individual source units, which  
335 have been identified as those sub-units (polygons) of the land-cover vector map consisting of  
336 natural forest or desert, or covered by cotton, jujube, cotton/ujube mixture. Two identifiers  
337 have been attributed to each source unit, (a) a metric coordinate whose numerical format re-  
338 fers to the corner of the corresponding polygon, and (b) a unique ID number followed by a de-  
339 scription of its land cover type. The soil NO source strength (i.e., actual NO flux, see Sect.  
340 2.2.4) of each source unit has been calculated from the corresponding net potential NO flux,  
341 the land-cover type specific gravimetric soil moisture content (“wilting point”), and the actual  
342 soil temperature, which has been *in-situ* measured for each of the land-cover types of Milan  
343 oasis (see Sect. 2.2.2). Those polygons which are not matching the mentioned land-cover  
344 types and other tiny polygons generated by digital image processing techniques were  
345 dismissed to avoid intricate geometric errors affecting NO emission data. In other words,  
346 these “other classes” were dissolved before performing LASAT analysis to avoid extreme  
347 values.

### 348 **2.2.7 Three dimensional distribution of NO concentrations by Lagrangian dispersion** 349 **modelling (LASAT)**

350 Having the actual NO source units of the Milan oasis available, the 3-D distribution of NO  
351 concentrations in the atmospheric boundary layer (0 – 1500 m a.gr.) over Milan oasis have  
352 been calculated by the Lagrangian dispersion model LASAT (German VDI Guidelines  
353 VDI3945, part 3; c.f. Janicke Consulting, 2011). LASAT is a state-of-the-art model, since (a)  
354 LASAT is one of those transport-dispersion models of air-pollution which is officially  
355 licensed for legal use of environmental issues (in Germany), and (b) among comparable  
356 micro-scale (e.g. street canyons) transport-dispersion models LASAT considers at least  
357 chemical transformations of 1<sup>st</sup> order and keeps nonetheless truly operational. Being a  
358 transport-dispersion-model, LASAT basically considers advection (“pixel cross-talk”)

359 [applying the 3D-continuity equation for any chosen tracer](#) (see [German VDI Guidelines](#)  
360 [VDI3945, part 3, cf. Janicke Consulting, 2011](#)). For that, pre-processing of meteorological pa-  
361 rameters (i.e. 3-D wind distributions, based on meteorological in-situ measurements, see Sect.  
362 2.2.2) and calculation of dispersion parameters ( $\sigma_y$ ,  $\sigma_z$ ) have to be performed. Unfortunately,  
363 it was difficult to obtain fine resolution using LASAT individually. Therefore, LASAT model  
364 was integrated with Geographic Information System (ArcGIS) by using an advanced module  
365 namely LASarc (IVU Umwelt GmbH, 2012). LASarc allowed us to calculate NO  
366 concentrations using relatively fine resolution of 30m×30m and taking the advantages of  
367 using integrated map colour scheme in ArcGIS. This module has been used to realize Milan  
368 oasis' complex NO source configuration and to setup calculations of LASAT.

369 The model was designed to calculate NO-concentrations at 16 different vertical layers (0–3,  
370 3–5, 5–10, 10–20, 20–30, 30–50, 50–70, 70–100, 100–150, 150–200, 200–300, 300–400,  
371 400–500, 500–700, 700–1000, and 1000–1500 m a.gr.). The horizontal resolution is 30 m, in  
372 x-direction (W-E) as well in y-direction (S-N), which results in 656 (x) and 381 (y) grids for  
373 the Milan oasis domain. LASAT's meteorological input data contain a variety of parameters,  
374 namely start and end time ( $T_1$ ,  $T_2$ ), wind speed ( $U_a$ ) and wind direction ( $R_a$ ) at anemometer  
375 height ( $H_a$ ), average surface roughness ( $Z_0$ ), and atmospheric stability (in terms of stability  
376 classes). These parameters have been provided in a time-dependent tabular form, up-dated  
377 every 30 minutes (except  $Z_0$ ). Average (30 min) wind speed and wind direction data have  
378 been calculated from *in-situ* measurements (1 min resolution, see Sect. 2.2.2).

379 LASAT's pre-processing module determines the vertical profile of wind speed according to  
380 the well-known logarithmic relation,

$$381 \quad U(z) = \frac{u_*}{k} \ln\left(\frac{z}{Z_0}\right) \quad (11)$$

382 where  $U(z)$  is the horizontal wind speed ( $\text{m s}^{-1}$ ) at height  $z$  (m),  $u_*$  is the friction velocity  
383 ( $\text{m s}^{-1}$ ),  $k$  is the dimensionless von Karman constant ( $= 0.4$ , Simiu and Scanlan, 1996), and  $Z_0$   
384 is the surface roughness length (m). LASAT's pre-processing module accepts only one indivi-  
385 dual value for  $Z_0$ ; nevertheless, the required mean value has been calculated from all  $Z_0$ 's of  
386 Milan oasis domain, which have been assigned to each of the sub-units (polygons) of the  
387 vector land-cover map (see Sect. 2.2.5). For individual  $Z_0$ 's, we calculated land-cover specific  
388 NDVI data (normalized differential vegetation index) from Landsat ETM+ image (141/033)

389 
$$NDVI = \frac{r_{NIR} - r_{RED}}{r_{NIR} + r_{RED}} \quad (12)$$

390 where *NIR* is the reflectance in the near-infrared bandwidth (0.77-0.90 μm) and *RED* is the  
 391 reflectance in the red bandwidth (0.63-0.69 μm). In Landsat ETM+ images, these correspond  
 392 to bands 4 and 3, respectively. Finally,  $r_{NIR}$  and  $r_{RED}$  are the corresponding ratios of reflected  
 393 and incident energy as a function of wavelength (see Chander and Markham, 2003). Then,  
 394 surface roughness grid data was estimated as:

395 
$$Z_0(x, y) = \exp(a_{xy} NDVI(x, y) + b_{xy}) \quad (13)$$

396 where  $a_{xy}$  and  $b_{xy}$  are constants, which are, according to Morse et al. (2000), derived from  
 397  $NDVI(x, y)$  and  $GPS(x, y)$  data for known sample pixels representing the earlier classified land-  
 398 cover types, namely natural forest, desert, cotton, jujube, and cotton/jujube mixture.  
 399 Corresponding land-cover type  $Z_0$ 's are 0.45, 0.01, 0.18, 0.26, and 0.22 m, respectively; the  
 400 required average value over the entire LASAT model domain results in  $Z_0 = 0.22 \pm 0.158$  m.

401 Besides mechanical turbulence ( $Z_0$ ), atmospheric stability affects most the dispersion of trace  
 402 substances. For Milan oasis' atmospheric boundary layer, atmospheric stability has been cal-  
 403 culated according to the "solar radiation/delta T (SRDT)" method in 30 min intervals. This  
 404 method (c.f. Turner, 1994) is widely accepted because of its simplicity and its representative-  
 405 ness for atmospheric stability over open country and rural areas, like the Milan oasis domain.  
 406 Daytime stability classes are calculated from *in-situ* measurements of solar radiation and  
 407 horizontal wind speed (see Sect. 2.2.2).

408 Finally, 30 min means of all parameters and input variables of LASAT have been calculated.  
 409 Using these, about  $4 \times 10^6$  gridded data points of 3-D NO concentration have been calculated  
 410 for each time period considered in Section 3.2.

#### 411 2.2.8 Simulation of $SCD_{NO_2}$ and $VCD_{NO_2}$ by spatial integration of LASAT results

412 There is only one tool to provide a robust relationship between biogenic soil NO emissions on  
 413 one hand and MAX-DOAS observed  $SCD$ 's and  $VCD$ 's on the other hand: the exact simula-  
 414 tion of the MAX-DOAS measurement through spatial integration of three dimensional NO  
 415 concentrations calculated by LASAT (followed by  $NO \rightarrow NO_2$  conversion). At a given  
 416 location of the MAX-DOAS measurement, integration must be performed from the height  
 417 where the MAX-DOAS instrument has been set-up ( $h_{MAXDOAS}$ ) to the end of the atmospheric  
 418 boundary layer ( $h_{ABL} = 1500$  m a.gr.) along two virtual light paths, (a) the vertical up path

419 (VCD), and (b) the slant path (SCD) according to the selected elevation angle of each MAX-  
 420 DOAS measurement.

421 Calculation of simulated VCD's for NO ( $VCD_{NO,sim}$ ) at the location of a MAX-DOAS  
 422 instrument is achieved as follows: (a) determination of the NO mass density ( $ng\ m^{-2}$ ) of the  
 423 vertical column between  $h_{MAXDOAS}$  and  $h_{ABL}$ ; this is obtained by adding NO concentrations  
 424 ( $ng\ m^{-3}$  in terms of mass of nitric oxide) of all LASAT cells in vertical direction over that  
 425  $30\ m \times 30\ m$  grid, which contains the location of the MAX-DOAS instrument, multiplied by  
 426 the height difference  $\Delta h = h_{ABL} - h_{MAXDOAS}$  (in m), (b) multiplying that NO mass density by  
 427 the ratio of Avogadro's number ( $6.02217 \times 10^{26}$  molecules  $kmol^{-1}$ ) and the molecular weight of  
 428 NO ( $30.0061 \times 10^{12}$   $ng\ kmol^{-1}$ ) delivers the desired value of  $VCD_{NO,sim}$  in units of molecules  
 429  $m^{-2}$  ( $\times 10^{-4}$ : molecules  $cm^{-2}$ ) at the location of the MAX-DOAS instrument. Calculation of  
 430 simulated SCD's for NO ( $SCD_{NO,sim}$ ) requires the determination of the 3-D light path through  
 431 the trace gas layered. Positioning of MAX-DOAS's telescope was always to the north, the  
 432 selected MAX-DOAS elevation angle  $\alpha$  and  $h_{ABI}$  deliver the length of the slant light path  
 433 ( $= h_{ABL}/\sin\alpha$ ). The desired  $SCD_{NO,sim}$  (in molecules  $m^{-2}$ ) results from the NO mass density of  
 434 the slant column multiplied by the length of the slant light path, where the NO mass density is  
 435 equivalent to the sum of all NO concentrations of those LASAT cells which are intersected by  
 436 the slant light path from the position of the MAX-DOAS instrument to  $h_{ABL}$ .

437 For conversion of  $VCD_{NO,sim}$  to  $VCD_{NO_2,sim}$  and  $SCD_{NO,sim}$  to  $SCD_{NO_2,sim}$  it is assumed, that  
 438 the photostationary state (PSS) of the triad NO, NO<sub>2</sub>, and O<sub>3</sub> is established in Milan oasis'  
 439 atmospheric boundary layer. According to Leighton (1961) this chemical equilibrium state is  
 440 due to fast photochemical reactions, namely  $NO+O_3 \rightarrow NO_2+O_2$  and  $NO_2+h\nu \rightarrow NO+O$ , from  
 441 which the so-called photostationary state NO<sub>2</sub> concentration ( $NO_{2,PSS}$ ) can be derived as

$$442 \quad [NO_{2,PSS}] = \frac{[O_3][NO]k_1}{j(NO_2)} \quad (14)$$

443 where  $[O_3]$  is the ozone number density (molecules  $cm^{-3}$ ; calculated from *in-situ* measured O<sub>3</sub>  
 444 concentrations, see Sect. 2.2.2),  $[NO]$  is the NO number density,  $k_1$  is the reaction coefficient  
 445 of the  $NO+O_3 \rightarrow NO_2+O_2$  reaction ( $cm^3\ molecules^{-1}\ s^{-1}$ ; Atkinson et al., 2004), and  $j(NO_2)$  is  
 446 the *in-situ* measured NO<sub>2</sub> photolysis rate (in  $s^{-1}$ ; see Sect. 2.2.2). Finally,  $VCD_{NO_2,sim}$  and  
 447  $SCD_{NO_2,sim}$  are calculated from  $VCD_{NO,sim}$  and  $SCD_{NO,sim}$  by

$$448 \quad VCD_{NO_2,sim} = CF_0 \times VCD_{NO,sim} \quad \text{and} \quad SCD_{NO_2,sim} = CF_0 \times SCD_{NO,sim} \quad (15)$$

449 where the NO→NO<sub>2</sub> conversion factor is defined by  $CF_0 = [O_3] k_1 / j(NO_2)$ .

450 Since the NO-NO<sub>2</sub>-O<sub>3</sub> photochemical equilibrium could not be handled by LASAT's  
451 "chemical" algorithm, we decided to use measured data (O<sub>3</sub> mixing ratio, NO<sub>2</sub> photolysis rate,  
452 s. sect. 2.2.2) to convert the calculated 3D-NO mixing ratio to the photo-stationary 3D-NO<sub>2</sub>  
453 mixing ratio. For that, a constant vertical O<sub>3</sub> mixing ratio (up to 1500 m a.gr.) is assumed over  
454 Milan oasis. This is justified by the fact, that particularly in arid and hyper-arid landscapes at  
455 mid-day conditions (maximum of insolation) the entire atmospheric boundary layer is  
456 intensively mixed, which is due to extensive convective heating of the surface by the sun  
457 which produces powerful buoyant thermals that establish the so-called mixing layer.  
458 Consequently an uniform vertical mixing ratio is expected for trace gases with chemical  
459 lifetimes greater than the exchange time of the atmospheric boundary layer. (c.f. Husar et al.  
460 1978, Stull 1988). This assumption is valid for ozone. Vertically constant O<sub>3</sub> mixing ratio  
461 has been reported for the atmospheric boundary layer over semi-arid southern Africa  
462 (Meixner et al., 1993). Concerning the vertical distribution of j(NO<sub>2</sub>) it is obvious, that the  
463 downward component of the actinic flux increases with increasing elevation due to the  
464 decreasing optical thickness of the scattering air masses. However, the altitude effect on the  
465 actinic flux in the first kilometer of the troposphere is typically very small. Trebs et al. (2009)  
466 used the Tropospheric Ultraviolet Visible model to calculate the typical vertical change of the  
467 actinic flux and found a vertical gradient of 1.1%/km. Consequently, our calculations of the  
468 NO to NO<sub>2</sub> conversion in the boundary-layer over Milan oasis (1500 m a.gr.) have not  
469 considered any potential vertical change of the j(NO<sub>2</sub>) values measured at ground level.

470 Nevertheless, for the case of our measurements the locally enhanced NO values caused by the  
471 soil emissions have a small but systematic effect on the ozone concentration, and thus also on  
472 the Leighton ratio: Close to the surface (below about 50m) the NO concentrations can be  
473 quite large, with maximum values up to about 10 ppb. Consequently, the ozone concentration  
474 will be reduced due to the reaction with NO by up to about 10 ppb. This means that the  
475 Leighton ratio will be reduced by up to about 25%. Although the reduction of the ozone  
476 mixing ratio will be partly compensated by mixing with air from higher altitudes, the  
477 simulated NO<sub>2</sub> mixing ratios might overestimate the true NO<sub>2</sub> mixing ratios by up to about  
478 25%. Probably the true overestimation for our measurements is much smaller because the  
479 typical NO mixing ratio within the lowest 100m is much lower than 10 ppb.

480

## 481 3 Results and Discussion

### 482 3.1 Land-cover type specific net potential NO fluxes

483 Net potential NO fluxes (as functions of soil temperature and moisture) have been determined  
484 by incubation of samples which have been taken from the top-soil of Milan oasis' major land-  
485 cover types, i.e. natural forest, desert, cotton, jujube, and cotton/ujube mixture (see Sect.  
486 2.2.4). Figure 2 shows the laboratory derived net potential ~~net~~-NO flux,  $F_{NO}$  from soils of the  
487 most contrasting land-cover types of Milan oasis (irrigated & fertilized fields of cotton,  
488 jujube, cotton/ujube mixture, and desert).

489 Net potential NO fluxes of the natural forest land-cover type are not shown, because  
490 laboratory incubation measurements have shown that there is no significant NO release from  
491 these soils, most likely due to its high electrical conductivity (salt content). Optimum  
492 gravimetric soil water contents (i.e., where the maximum of  $F_{NO}$  is observed) for desert,  
493 managed cotton, and managed jujube soils have one in common, very low values of  $\theta_{g,opt}$   
494 (0.009–0.017) for soil temperatures of 50°C. During the vegetation period (April –  
495 September), soil temperatures of > 40°C are easily reached for the soils of Milan oasis,  
496 particularly for the desert soils. While the nature of all Milan oasis' soils is arid/hyper-arid,  
497 maximum net potential NO fluxes are 7600, 63, 270, and 98 ng m<sup>-2</sup> s<sup>-1</sup> (in terms of mass of  
498 nitric oxide) for cotton, jujube, jujube/cotton mixture, and desert soils, respectively.

### 499 3.2 Land-cover types of Milan oasis and actual NO fluxes

500 As mentioned in Section 2.2.5, land-cover classification and actual distribution of Milan  
501 oasis' fields have been identified from satellite images (Quickbird, Landsat ETM+). The 2011  
502 distribution of fields and the corresponding land-cover is shown in Figure 3.

503 The dominant crop was cotton, representing 18% (64 km<sup>2</sup>) of the total field area of Milan  
504 oasis (jujube 7%, 28 km<sup>2</sup>), cotton/ujube mixture 0.89 % (3 km<sup>2</sup>), natural forest 18% (64 km<sup>2</sup>),  
505 residential area 1.62% (5.5 km<sup>2</sup>) and desert 52% (174 km<sup>2</sup>). Land-cover specific, actual NO  
506 fluxes (30 min means) from cotton, jujube, cotton/ujube, and desert soils were calculated  
507 from corresponding laboratory derived net potential NO fluxes, land-type specific soil  
508 moisture and soil temperature data (see Sect. 2.2.6). These NO fluxes (ng m<sup>-2</sup> s<sup>-1</sup>, in terms of  
509 mass of nitric oxide) were then assigned to each individual source unit (i.e. to each of the  
510 2500 polygons of Milan oasis' domain).

511 For the period 03 to 24 June, 2011, land-cover specific, actual NO fluxes were calculated

512 according to eq.(10) for cotton, jujube, cotton/ujube, and desert soils from corresponding  
513 laboratory derived net potential NO fluxes. As input we used land-type specific, measured  
514 soil temperature data as well as land-type specific soil moisture data (so-called “wilting  
515 points”, s. Sect. 2.2.3). The calculated NO fluxes are shown in Fig. 4 as median diel variation  
516 (for the entire period of 03 to 24 June, 2011). Since NO fluxes from Milan cotton fields  
517 dominate the total soil biogenic NO emission of the oasis, corresponding medians and  
518 quartiles are shown in Fig. 4, while – for the sake of clarity – for jujube, cotton/ujube, and  
519 desert only medians are given. Since land-type specific “wilting points” are constant, diel  
520 variations of actual NO fluxes mirror directly those of corresponding soil temperatures,  
521 showing the daily minimum around 06:00 local time for all four major land-cover types. The  
522 maximum of the actual NO-flux, however, is around 13:00 (local time) for jujube,  
523 cotton/ujube, and desert soils, and 15:00 local time for cotton. This is due to the growth of  
524 the cotton plants: while at the beginning of the experimental period the bare soil surface was  
525 nearly 100% exposed to insolation, the growing cotton canopy has shaded great parts of the  
526 soil surface-towards the end of the experimental period . This is also reflected by the skewed  
527 distribution of actual NO-fluxes from cotton covered soil, indicated by the daytime non-  
528 symmetric inter-quartile range (= upper quartile – lower quartile). As shown in sect. 3.5,  
529 actual NO-flux data of 09 June, 2011 (08:30-14:30 local time) were used for the comparison  
530 of LASAT and MAX-DOAS results. During this particular day (within the first week of the  
531 experimental period), the derived flux for “land-cover cotton” ranged from 15–64 ng m<sup>-2</sup>s<sup>-1</sup>  
532 (in terms of mass of NO), those for jujube, cotton/ujube, and desert land-covers ranged from  
533 11–13, 6–16, and 6–17 ng m<sup>-2</sup>s<sup>-1</sup>, respectively. These actual NO fluxes were then assigned to  
534 each individual source unit (i.e. to each of the 2500 polygons of Milan oasis’ domain). The  
535 soil biogenic NO emission from all cotton fields between 08:30 and 14:30 was estimated to  
536 28.7 kg (in terms of mass of NO), equivalent to 76% of the total soil biogenic NO emission of  
537 the entire Milan oasis within 6 hours.

### 538 **3.3 Vertical NO<sub>2</sub> column densities by MAX-DOAS**

539 We performed 32 individual MAX-DOAS measurements within 21 days of the 2011 field  
540 campaign to examine the spatial variation between the observed sites. In Fig. 5, all observed  
541 vertical NO<sub>2</sub> column densities (in molecules cm<sup>-2</sup>) observed at sites (1) - (4) of Milan oasis are  
542 shown in polar coordinates with reference to corresponding wind directions measured *in-situ*  
543 at the individual sites.

544 Wind speeds (30 min means) ranged between 1.5 and 7.7 m s<sup>-1</sup> and wind direction was mostly  
545 (78%) from the northern quadrants (59%, 9%, 13%, and 19% from NE, SE, SW, and NE  
546 quadrants, respectively). As expected, highest VCDs (10<sup>15</sup> – 10<sup>16</sup> molecules cm<sup>-2</sup>) were  
547 observed at site (4) (Milan oasis center), regardless of wind direction. When the wind  
548 direction is from the NE quadrant, site (3) (jujube fields) is down-wind of Milan oasis (see  
549 Fig.1); then its VCDs are as high as those obtained in the oasis' center (5 – 7×10<sup>15</sup> molecules  
550 cm<sup>-2</sup>). The few VCD data points of 1×10<sup>15</sup> molecules cm<sup>-2</sup> at the jujube site, attributed to  
551 winds from SE and SW quadrants, are mainly due to NO emissions from traffic on the  
552 National Road 315 which passes the southern margins of Milan oasis. Lowest VCDs  
553 (3×10<sup>13</sup> – 3×10<sup>14</sup> molecules cm<sup>-2</sup>) have been observed at site (1) (natural forest) and site (2)  
554 (desert). Alone from these spatially resolved VCD observations in the Milan oasis' domain,  
555 the increase of VCD due to the oasis itself can be estimated in the order of at least one order  
556 of magnitude.

557 Fortunately, we have been able to perform simultaneous measurements with two MAX-  
558 DOAS instruments at sites (1) and (3) on 09 and 13 June, 2011. Since winds (approx. 3 m s<sup>-1</sup>)  
559 were from the NE quadrant during these two days, site (1) has been up-wind, and site (3)  
560 downwind of Milan oasis. Corresponding VCD results are shown in Figure 6. NO<sub>2</sub> VCDs at  
561 the downwind site exceeded those at the upwind site by factors 5 – 9. This difference between  
562 downwind and upwind MAXDOAS signals is considered to be a direct measure for the areal  
563 increase of ambient NO<sub>2</sub> concentration. In the absence of anthropogenic NO<sub>x</sub> sources (see  
564 Sect. 2.1), this provides first evidence for the considerable impact of the biogenic NO emissi-  
565 ons from the fields of Milan oasis.

### 566 3.4 3-D distribution of ambient NO-concentration

567 The LASAT model has to be used to calculate the dispersion of soil emitted NO into the at-  
568 mospheric boundary layer over Milan oasis. An example for the resulting distribution of NO  
569 the concentration in the first four vertical layers of LASAT (0-3, 3-5, 5-10, and 10-20 m) is  
570 shown in Figure 7 (09 June, 2011; 11:30-13:00 local time). The shown results are the mean of  
571 three LASAT model runs, since a new LASAT calculation of 3-D distribution of NO  
572 concentration is started for every set of meteorological parameters which are provided every  
573 30 min from means of the *in-situ* measured meteorological quantities (see Sect. 2.2.2). During  
574 11:30-13:00, mean wind direction was 15°, 38°, and 50°, wind speed was rather constant  
575 (2.60 – 2.67 m s<sup>-1</sup>), and atmospheric stability class has been generally neutral (3.2).

576 By comparing the NO ambient concentrations, particularly in the first vertical LASAT layer  
577 (0–3 m) of oasis area with the surrounding desert, it becomes obvious that the great differ-  
578 ences of ambient NO concentrations mirror the corresponding differences of actual soil NO  
579 fluxes from each source-unit; within this layer calculated mean NO concentrations are 13, 12,  
580 10, and 1 ng m<sup>-3</sup> (in terms of mass of nitric oxide; or 10.6, 9.8, 8.2, and 0.8 ppb) for the oasis  
581 centre, jujube fields, cotton/jujube mixture, and desert, respectively. The value at the oasis  
582 center exceeds those over desert by more than an order of magnitude, similar as the  
583 corresponding VCD values (see above). As expected under the prevailing conditions of well  
584 developed atmospheric turbulence, NO concentrations rapidly decreases with height (see  
585 panels “0–3 m”, “3–5 m”, “5–10 m” in Fig. 7), and with prevailing northerly winds, the NO  
586 concentration centre shifting southwards with increasing altitude.

### 587 3.5 Simulated SCDs and VCDs vs. SCDs and VCDs by MAX-DOAS

588 For those periods where simultaneous “upwind” and “downwind” MAX-DOAS  
589 measurements have been performed (09 and 13 June, 2011), corresponding SCD<sub>sim</sub> and  
590 VCD<sub>sim</sub> have been simulated by suitable vertical integration (see Sect. 2.2.8) of LASAT-  
591 calculated 3-D NO concentrations, followed by NO→NO<sub>2</sub> conversion (based on  
592 photostationary state assumption of Milan oasis’ atmospheric boundary layer). Since SCD<sub>sim</sub>  
593 and VCD<sub>sim</sub> represent only that part of true SCDs and VCDs of NO<sub>2</sub>, which are due to the  
594 contribution of the oasis’ soil NO emissions, SCD<sub>sim</sub> and VCD<sub>sim</sub> are compared to the  
595 difference of those SCDs and VCDs which have been simultaneously measured by two  
596 MAX-DOAS instruments at corresponding “downwind” and “upwind” sites (see Fig. 8). For  
597 elevation angles of 2° and 4°, SCD<sub>sim</sub> and  $\Delta\text{SCD} = \text{SCD}_{\text{down}} - \text{SCD}_{\text{up}}$  are shown in Figure 8a.  
598 In Figure 8b, VCD<sub>sim</sub> and  $\Delta\text{VCD} = \text{VCD}_{\text{down}} - \text{VCD}_{\text{up}}$  are shown for 15° elevation.

599 Here it should be noted that in principle the accuracy of the geometric approximation is  
600 higher for the high elevation angles than for the lower elevation angles. However, for the  
601 specific cases studied here, this is not the case. First, close to the sources, the height of the  
602 layer with elevated NO<sub>2</sub> is quite low (in our case the bulk of NO<sub>2</sub> is located below 100 m).  
603 Second, also the aerosol load is usually very low. Thus the probability of scattering events  
604 inside the layer of enhanced NO<sub>2</sub> is very low, and consequently the accuracy of the geometric  
605 approximation is relatively high. To further quantify the associated uncertainties, we  
606 performed radiative transfer simulations and found that the deviations from the geometric  
607 approximation are similar for the different elevation angles (about 5% for 2°, 3% for 4° and  
608 3% for 15°). However, because of the shorter light paths through the NO<sub>2</sub> layer, the relative

609 error caused by the uncertainty of the spectral analysis is higher than for the low elevation  
610 angles. Thus for the case of our measurements, we indeed expect lower uncertainties for the  
611 low elevation angles.

612 Since soil NO emission data used in the LASAT dispersion model were calculated from land-  
613 cover type specific potential net NO fluxes, which in turn were derived from laboratory  
614 incubation experiments on corresponding soil samples, the results in Figure 8 are also  
615 considered as an excellent quality assurance of the chosen up-scaling of laboratory results to  
616 the oasis scale. There is remarkable good agreement between measured and simulated data.

617 However, the actual NO emissions (irrespective of the land-cover type) have their maximum  
618 in the early afternoon (s. Fig. 4), while the highest height-integrated NO<sub>2</sub> concentrations as  
619 simulated by LASAT (on the basis of the actual NO emissions) are in the morning (08:30–  
620 10:00), followed by rather constant values for the remainder of the day (s. Fig. 8). The apparent  
621 discrepancy between both diurnal variations can be simply explained by the diurnal variation  
622 of the wind direction and the specific viewing geometry of the MAX-DOAS instrument. The  
623 MAX-DOAS instrument was located at the south-west corner of the oasis, and the  
624 observations at zenith and low elevation angles probed air masses located at different  
625 locations across the oasis. The wind direction was from north-east in the morning and turned  
626 to north-west in the afternoon. Hence, air masses of lower concentration crossed the viewing  
627 directions in the afternoon compared to those in the morning. This explains that in spite of the  
628 larger NO<sub>x</sub> emissions smaller column densities have been observed in the afternoon. The  
629 apparent discrepancy of the diurnal cycles of NO emissions and measured NO<sub>2</sub> column  
630 densities indicates the importance to exactly consider the 3-dimensional NO<sub>2</sub> distribution (due  
631 to the soil-emitted NO) for the comparison of the model results with MAX-DOAS  
632 observations.

633 The Figure 8b shows that the LASAT simulations overestimate slightly the true NO<sub>2</sub> VCD.  
634 The both measured and simulated NO<sub>2</sub> VSDs have with an average root mean square (RMS)  
635 error between the measured and simulated values of approx. 5-15%. However, the  
636 overestimation of LASAT simulation is well suited to the fact that in reality a little less NO  
637 can be converted to the NO<sub>2</sub> because of lower ozone concentration at the surface.

638

#### 639 **4 Conclusion**

640 This study has been focused on the following activities: (1) representative soil sampling from  
641 the uppermost soil layer (< 0.05 m) of all land-cover type units (natural forest, cotton fields,

642 jujube fields, cotton/jujube mixture, desert) of Milan oasis (Xinjiang, NW China), (2) labora-  
643 tory incubation experiments (dynamic chamber system) to characterize the biogenic NO emis-  
644 sion from these soil samples in form of net potential NO fluxes as function of soil moisture  
645 and soil temperature, (3) determination of the actual size, areal distribution, and land-cover  
646 type of Milan oasis' field units from satellite remote sensing information, (4) field measure-  
647 ments of slant (SCD) and vertical (VCD) NO<sub>2</sub> column densities (by MAX-DOAS) and  
648 additional quantities (soil moisture, soil temperature, ozone concentration, NO<sub>2</sub> photolysis  
649 rate, meteorological parameters) during an extended field campaign of 4 weeks at Milan oasis,  
650 (5) using data from (2), (3) and (4): calculation of Milan oasis' 2D distribution of actual, land-  
651 cover specific NO fluxes, (6) calculation of 3-D NO concentrations in Milan oasis' atmosphe-  
652 ric boundary layer originating from the dispersion of biogenic NO soil emissions determined  
653 by (5) with help of the Lagrangian dispersion model LASAT, (7) simulation of SCDs and  
654 VCDs by suitable vertical integration of calculated 3-D NO concentrations followed by  
655 suitable NO→NO<sub>2</sub> conversion factors derived from *in-situ* measurements, (8) comparison of  
656 measured and simulated SCDs and VCDs.

657 Results of the laboratory derived NO fluxes have shown that the extensively managed (fertiliz-  
658 ed and efficiently irrigated) cotton fields of Milan oasis release large amounts of soil bio-  
659 genic NO; NO fluxes range between 10–30 ng m<sup>-2</sup> s<sup>-1</sup> (in terms of mass of N), that is approx.  
660 5–10 times more than from a typical central European wheat field ([Yamulki et al. 1995; Stohl](#)  
661 [et al. 1996](#)).

662 Applying two MAX-DOAS instruments, simultaneous measurements have been performed at  
663 upwind and downwind sites of Milan oasis. Downwind site VCDs exceeded those from the  
664 upwind site by factors 5 – 9. Differences of VCD and SSC (“downwind” minus “upwind”) are  
665 a direct measure for the areal increase of ambient NO<sub>2</sub> concentration caused by the oasis  
666 itself. The measured differences of VCDs and SCDs were compared with the simulated VCDs  
667 and SCDs and excellent agreement was found.

668 This agreement is considered as the first successful attempt to prove the validity of the chosen  
669 approach to up-scale laboratory derived biogenic NO fluxes to ecosystem level field con-  
670 ditions, i.e. from the spatial scale of a soil sample (cm<sup>2</sup>) to field size (ha), and from field size  
671 (ha) to the size of an entire (agro-) ecosystem (km<sup>2</sup>). Furthermore, in the absence of anthropo-  
672 genic NO sources of Milan oasis (hydropower energy, battery powered trikes), it is obvious,  
673 that the areal increase of ambient NO<sub>2</sub> concentration in the atmospheric boundary layer of the  
674 isolated (in terms of NO<sub>2</sub> advection) Milan oasis is entirely due to biogenic NO emission from  
675 the arid/hyper-arid soils of the oasis itself. Extensive agricultural management of Milan oasis'

676 crop fields (fertilization (350- 600 kg N ha<sup>-1</sup>a<sup>-1</sup>) and effective irrigation of cotton and jujube  
677 fields) obviously provides considerable contribution of biogenic NO<sub>x</sub> (NO+NO<sub>2</sub>) from  
678 arid/hyper-arid soils of the Taklimakan desert to the local tropospheric NO<sub>x</sub> budget.  
679 About 80% of the Chinese cotton production originates from the 3000 km long belt of oases  
680 surrounding Taklimakan Desert (1.65×10<sup>6</sup> km<sup>2</sup>) in Xinjiang (NW-China); cotton cultivated  
681 land area in Xinjiang occupies the first place of entire China. Since 1955, Xinjiang's output of  
682 cotton increased 294 times (Lei et al., 2005). Fast economic growth in the region (+11% GDP  
683 a<sup>-1</sup>), inevitably accompanied by large anthropogenic NO<sub>x</sub> emissions (traffic, energy producti-  
684 on), may be countervailed or even exceeded by the “hotspot” character of Xinjiang’s oases,  
685 namely by soil biogenic NO emissions from agriculturally dominated oases. Most likely, they  
686 will contribute most to the regional tropospheric NO<sub>x</sub> budget. This is all the more likely,  
687 given the continued intensification of oasis agriculture around the Taklimakan desert which  
688 will be accompanied by corresponding land use change (desert→dryland farming with  
689 irrigation) in the coming decades.

#### 690 **Acknowledgements**

691 This work was funded through the German Research Foundation (DFG) project “DEQNO –  
692 Desert Encroachment in Central Asia – Quantification of soil biogenic Nitric Oxide” (DFG-  
693 MA 4798/1-1), the Max Planck Society (MPG), and the Max Planck Graduate Centre with  
694 Johannes Gutenberg-University Mainz (MPGC). The authors like to thank Guozheng Song,  
695 Günter Schebeske, Achim Zipka, Yanhong Li, Fanxia Wang, Aixia Yang, Sijun Luo, and  
696 Zhilin Zhu for their field assistance and their substantial support before, during, and after the  
697 DEQNO 2011 campaign. We also thank Reza Shaiganfar and Steffen Beirle for their supports  
698 during the pre-preparation of MAX-DOAS instrument.

699

700

701

Formatted: German (Germany)

702 **References:**

- 703 Ashuri, F.A.: Der Austausch von Stickstoffmonoxid zwischen Boden und Atmosphäre unter  
704 besonderer Berücksichtigung des Bodenwassergehaltes, Einfluss kulturnaturlandschaftlicher  
705 Verhältnisse auf den Umsatz eines Spurengases. Ph.D. thesis, Johannes Gutenberg  
706 University Mainz, Mainz, Germany, 1–169, 2009.
- 707 Atkinson, R., Baulch, D.L., Cox, R.A., Crowley, J.N., Hampson, R.F., Hynes, R.G., Jenkin,  
708 M.E., Rossi, M.J., Troe, J.: Evaluated kinetic and photochemical data for atmospheric  
709 chemistry: Volume I - Gas phase reactions of Ox, HOx, NOx and SOx species, *Atmos.*  
710 *Chem. Phys.*, 4, 1461–1738, 2004.
- 711 Bargsten, A., Falge, E., Pritsch, K., Huwe, B., Meixner, F.X.: Laboratory measurements of  
712 nitric oxide release from forest soil with a thick organic layer under different understory  
713 types, *Biogeosciences*, 7, 1425–1441, 2010.
- 714 Behrendt, T., Veres, P.R., Ashuri, F., Song, G., Flanz, M., Mamtimin, B., Bruse, M.,  
715 Williams, J., Meixner, F.X.: Characterisation of NO production and consumption: new in-  
716 sights by an improved laboratory dynamic chamber technique, *Biogeosciences Discuss.*,  
717 11, 1187–1275, 2014.
- 718 Beirle, S., Platt, U., Wenig, M. and Wagner, T.: Highly resolved global distribution of  
719 tropospheric NO<sub>2</sub> using GOME narrow swath mode data, *Atmos. Chem. Phys.*, 4, 1913–  
720 1924, 2004.
- 721 Bogumil, K., Orphal, J., Homann, T., Voigt, S., Spietz, P., Fleischmann, O.C., Vogel, A.,  
722 Hartmann, A., Kromminga, H., Bovensmann, H., Frerick, J., Burrows, J.P.: Measurements  
723 of molecular absorption spectra with the SCIAMACHY pre-flight model: instrument  
724 characterization and reference data for atmospheric remote-sensing in the 230–2380 nm  
725 region, *Journal of Photochemistry and Photobiology A-chemistry*, 157(2), 167–184, 2003.
- 726 Brinksma, E. J., Pinardi, G., Volten, H., Braak, R., Richter, A., Schoenhardt, A., Van  
727 Roozendaal, M., Fayt, C., Hermans, C., Dirksen, R. J., Vlemmix, T., Berkhout, A.J.C.,  
728 Swart, D.P. J., Oetjen, H., Wittrock, F., Wagner, T., Ibrahim, O. W., Leeuw, G. de.,  
729 Moerman, M., Curier, R. L., Celarier, E. A., Cede, A., Knap, W. H., Veefkind, J. P.,  
730 Eskes, H. J., Allaart, M., Rothe, R., Pitters, A. J. M., Levelt, P. F.: The 2005 and 2006  
731 DANDELIONS NO<sub>2</sub> and aerosol intercomparison campaigns, *Journal of Geophysical*  
732 *Research*, Vol. 113, 1–18, 2008.
- 733 Chameides, W. L., Fehsenfeld, F., Rodgers, M. O., Cardelino, C., Martinez, J., Parrish, D.,  
734 Lonneman, W., Lawson, D. R., Rasmussen, R. A., Zimmerman, P., Greenberg, J.,  
735 Middleton, P., Wang, T.: Ozone precursor relationships in the ambient atmosphere, *Journal*  
736 *of Geophysical Research*, 92, 6037–6055, 1992.
- 737 Chander, G. and Markham, B.: Revised Landsat-5 TM radiometric calibration procedures and  
738 postcalibration dynamic ranges, *IEEE Transactions on Geoscience and Remote Sensing*, 41  
739 (11), 2674–2677, 2003.
- 740 Conrad, R.: Soil Microorganisms as controllers of atmospheric trace gases (H<sub>2</sub>, CO, CH<sub>4</sub>,  
741 COS, N<sub>2</sub>O and NO), *Microbiological Reviews.*, 60 (4), 609–640, 1996.
- 742 Crutzen, P. J. (1987): Role of the tropics in atmospheric chemistry, in: *The Geophysiology of*  
743 *Amazonia*, Dickinson, R.E. (ed.), pp. 107–132, 1987, John Wiley & Sons, New York.
- 744 Davidson, E. A., Kinglerlee, W.: A global inventory of nitric oxide emissions from soils,  
745 *Nutrient Cycling in Agroecosystems*, 48, 37–50, 1997.
- 746 Denman, K.L., Brasseur, G.P., Chidthaisong, A., Ciais, P., Cox, P.M., Dickinson, R.E.,  
747 Hauglustaine, D., Heinze, C., Holland, E.A., Jacob, D.J., Lohmann, U., Ramachandran,  
748 S., Da Silva Dias, P.L., Wofsy, S.C., Zhang, X.: Couplings between changes in the climate  
749 system and biogeochemistry, in *Climate Change 2007: The physical science basis.*  
750 contribution of working group 1 to the fourth assessment report of the Intergovernmental

751 Panel on Climate Change, edited by Solomon, S., Qin, D., Manning, M., Chen, Z.,  
752 Marquis, M., Averyt, K.B., Tignor, M., Miller, H.L., Cambridge University Press,  
753 Cambridge, 499-588, 2007.

754 Feig, G.T.: Soil Biogenic Emissions of Nitric Oxide from Arid and Semi-Arid Ecosystems,  
755 PhD thesis, Johannes Gutenberg University Mainz, Mainz, Germany, 1–222, 2009.

756 Feig, G.T., Mamtimin, B., Meixner, F. X.: Soil biogenic emissions of nitric oxide from a  
757 semi-arid savanna in South Africa, *Biogeosciences*, 5, 1723–1738, 2008a.

758 Feig, G.T., Mamtimin, B., Meixner, F. X.: Use of laboratory and remote sensing techniques to  
759 estimate vegetation patch scale emissions of nitric oxide from an arid Kalahari savanna,  
760 *Biogeosciences Discuss.*, 5, 4621–4680, 2008b.

761 Galbally, I.E., Johansson, C.: A model relating laboratory measurements of rates of nitric  
762 oxide production and field measurements of nitric oxide emissions from soils, *Journal of*  
763 *Geophysical Research*, 94, 6473- 6480, 1989.

764 Ganzeveld, L., Eerdeken, G., Feig, G.T., Fischer, H., Harder, H., Königstedt, R., Kubistin,  
765 D., Martinez, M., Meixner, F.X., Scheeren, B., Williams, J., Lelieveld, J.: Boundary layer  
766 exchanges of volatile organic compounds, nitrogen oxides and ozone during the GABRIEL  
767 campaign, *Atmospheric Chemistry and Physics*, 8, 6223-6243, 2008.

768 Gelfand, I., Feig, G., Meixner, F.X., Yakir, D.: Afforestation of semi-arid shrubland reduces  
769 biogenic NO emission from soil, *Soil Biology and Biochemistry* 41, 1561–1570, 2009.

770 Harrison, P., Pearce F.: *Deserts and Drylands*, AAAS Atlas of Population and Environment,  
771 pp. 131-134, 2000. University of California Press, Berkeley, USA.

772 Hartge, H., Horn, R.: *Die physikalische Untersuchung von Böden: Praxis Messmethoden*  
773 *Auswertung*. Schweizerbart-sche Verlagsbuchhandlung, Stuttgart, 1-178, 2009.

774 Hermans, C., Vandeale, A.C., Carleer, M., Fally, S., Colin, R., Jenouvrier, A., Coquart, B.,  
775 Merienne, M. F.: Absorption Cross-Sections of Atmospheric Constituents, NO<sub>2</sub>, O<sub>2</sub>, and  
776 H<sub>2</sub>O, *Environ. Sci. Pollut. Res.*, 6, 151-158, 1999.

777 Hönninger, G. and Platt, U.: The Role of BrO and its Vertical Distribution during Surface  
778 Ozone Depletion at Alert, *Atmos. Environ.*, 36, 2481–2489, 2002.

779 Hönninger, G., von Friedeburg, C., and Platt, U.: Multi Axis Differential Optical Absorption  
780 Spectroscopy (MAX-DOAS), *Atmos. Chem. Phys.*, 4, 231–254, 2004.

781 [Husar, R.B., Patterson, D.E., Husar, J.D., Gillani, N.V., Wilson Jr., W.E. \(1978\), Sulfur](#)  
782 [budget of a power plant plume. \*Atmospheric Environment\*, 12 \(1-3\), 549-568.](#)

783 IVU Umwelt GmbH: LASarc – GIS integration of LASAT, Environmental Planning and  
784 Information Systems, Freiburg, Germany, 2012.

785 Janicke Consulting: Dispersion model LASAT, Version 3.2, Reference Book. Janicke  
786 Consulting, Überlingen, Germany, 239 p, 2011.

787 Kargas, G., Ntoulas, N., Nektarios, P.A.: Soil texture and salinity effects on calibration of  
788 TDR300 dielectric moisture sensor. *Soil Research*, 51 (4), 330-340, 2013.

789 Kirkman, G.A., Yang, W.X., Meixner, F.X.: Biogenic nitric oxide emissions upscaling: An  
790 approach for Zimbabwe, *Global Biogeochem. Cycles*, 15, 1005–1020, 2001.

791 Koeppen, W.: *Grundriss der Klimakunde*. Gruyter Verlag, Berlin/Leipzig, Germany, 388 p,  
792 1931.

793 [Kottek, M., Grieser, J., Beck, C., Rudolf, B. and Rubel, F.: \*World Map of the Köppen-Geiger\*](#)  
794 [\*climate classification Updated, \*Meteorologische Zeitschrift\*, 15 \(3\), 259-263, 2006.\*](#)

795 Kurucz, R. L., Furenlid, I., Brault, J., Testerman, L.: *Solar Flux Atlas from 296 nm to 1300*  
796 *nm*, National Solar Observatory Atlas No. 1, 1984. Office of University publisher, Harvard  
797 University, Cambridge.

- 798 Lei, J., Zhang, X. L.: Structural Adjustment of Oasis Agriculture in Xinjiang, Chinese Journal  
799 of Population, Resources and Environment, 3 (3), 29-33, 2005.
- 800 Leighton, P. A.: Photochemistry of Air Pollution, Academic Press, New York and London,  
801 300 p, 1961.
- 802 Leue, C., Wenig, M., Wagner, T., Platt, U., Jähne, B.: Quantitative analysis of NO<sub>x</sub> emissions  
803 from GOME satellite image sequences, J. Geophys. Res., 106, 5493-5505, 2001.
- 804 Ludwig, J., Meixner, F.X., Vogel, B., Förstner, J.: Processes, influencing factors, and  
805 modelling of nitric oxide surface exchange—an overview, Biogeochemistry, 52 (3), 225-  
806 257, 2001.
- 807 Mayer, J.-C., Bargsten, A., Rummel, U., Meixner, F.X., Foken, T.: Distributed modified  
808 Bowen ratio method for surface layer fluxes of reactive and non-reactive trace gases,  
809 Agricultural and Forest Meteorology, 151, 655-668, 2011.
- 810 [Meixner, F.X., Ajavon, A.-L., Helas, G., Scharffe, D., Zenker, T., Harris, G.W., Andreae,](#)  
811 [M.O. \(1993\). Vertical distribution of ozone over southern Africa: Airborne measurements](#)  
812 [during SAFARI-92, AGU Fall Meeting, San Francisco, U.S.A.](#)
- 813 Meixner, F.X., Yang, W.X.: Biogenic emissions of nitric oxide and nitrous oxide from arid  
814 and semiarid land, in: Dryland Ecohydrology, edited by: D'Odorico, P. and Porporat, A.,  
815 Springer, Dordrecht, the Netherlands, 233–255, 2006.
- 816 Morse, A., Tasumi, M., Allen, R. G., and Kramber, W. J. (2000): Application of the SEBAL  
817 Methodology for Estimating Consumptive Use of Water and Streamflow Depletion in the  
818 Bear River Basin of Idaho through Remote Sensing, Final report submitted to The  
819 Raytheon Systems Company, Earth Observation System Data and Information System  
820 Project, Boise, USA, 107 pp., 2000.
- 821 Otter, L.B., Yang, W.X., Scholes, M.C., Meixner, F. X.: Nitric Oxide emissions from a  
822 southern African Savannah, J. Geophys. Res., 104, 18471–18485, 1999.
- 823 Perumal, K. and Bhaskaran, R.: Supervised classification performance of multispectral  
824 images. Journal of Computing, 2-2, 124-129, 2010.
- 825 [Platt, U. and Stutz, J.: Differential Optical Absorption Spectroscopy: Principles and](#)  
826 [Applications, Springer, Berlin, Heidelberg, Germany, 135–377, 2008.](#)
- 827 Rothman, L.S., Jacquemart, D., Barbe, A., Chris Benner, D., Birk, M., Brown, L.R., Carleer,  
828 M.R., Chackerian Jr, C., Chance, K., Coudert, L.H., Dana, V., Devi, V.M., Flaud, J.-M.,  
829 Gamache, R.R., Goldman, A., Hartmann, J.-H., Jucks, K.W., Maki, A.G., Mandin, J.-Y.,  
830 Massie, S.T., Orphal, J., Perrin, A., Rinsland, C.P., Smith, M.A.H., Tennyson, J.,  
831 Tolchenov, R.N., Toth, R.A., Vander Auwera, J., Varanasi, P., Wagner, G.: The HITRAN  
832 2004 molecular spectroscopic database, Journal of Quantitative Spectroscopy & Radiative  
833 Transfer, 96, 139-204, 2005.
- 834 Rudolph, J., Conrad, R.: Flux between soil and atmosphere, vertical concentration profiles in  
835 soil, and turnover of nitric oxide: 2. Experiments with naturally layered soil cores, Journal  
836 of Atmospheric Chemistry, 23, 275-300, 1996.
- 837 Rudolph, J., Rothfuss, F., Conrad, R.: Flux between soil and atmosphere, vertical  
838 concentration profiles in soil, and turnover of nitric oxide: 1. Measurements on a model  
839 soil core, Journal of Atmospheric Chemistry, 23, 253–273, 1996.
- 840 Richter, A., Burrows, J.P.: Tropospheric NO<sub>2</sub> from GOME Measurements, Adv. Space Res.,  
841 29(11), 1673-1683, 2002.
- 842 Simiu, E., Scanlan, R.H.: Wind Effects on Structures: Fundamentals and Applications to  
843 Design, Third Edition, John Wiley & Sons, New York, USA, 704 p., 1996.

844 Sinreich, R., Frieß, U., Wagner, T., Platt, U.: Multi axis differential optical absorption  
845 spectroscopy (MAX-DOAS) of gas and aerosol distributions, *Faraday Discuss.*, 130, 153–  
846 164, doi:10.1039/b419274p, 2005.

847 Solomon, S., Schmeltekopf, A. L., Sanders, R. W.: On the interpretation of zenith sky  
848 absorption measurements, *J. Geophys. Res.*, 92, 8311–8319, 1987.

849 [Stohl, A., Williams, E., Wotawa, G. and Kolb, H.K.: A European Inventory of Soil Nitric  
850 Oxide Emissions and the Effect of these Emissions on the Photochemical Formation of  
851 Ozone, \*Atmospheric Environment\*, 30 \(22\), 3741–3755, 1996.](#)

852 [Stull, R.B. \(1988\), An Introduction to Boundary-Layer Meteorology, Kluwer Academic  
853 Publishers, Dordrecht, The Netherlands.](#)

854 [Trebs, I., Bohn, B., Ammann, C., Rummel, U., Blumthaler, M., Königstedt, R., Meixner, F.  
855 X., Fan, S., Andreae, M.O. \(2009\), Relationship between the NO<sub>2</sub> photolysis frequency  
856 and the solar global irradiance, \*Atmospheric Measurement Techniques\*, 2, 725–739](#)

857 Turner, D.B.: Workbook of atmospheric dispersion estimates. 2nd ed., Lewis publisher,  
858 London, 175 p, 1994.

859 van Dijk, S., Meixner, F.X.: Production and consumption of NO in forest and pasture soils  
860 from the amazon basin, *Water Air Pollut.-Focus*, 1, 119–130, 2001.

861 van Dijk, S.M., Gut, A., Kirkman, G.A., Meixner, F. X., Andreae, M.O., Gomes, B. M.:  
862 Biogenic NO emissions from forest and pasture soils: relating laboratory studies to field  
863 measurements, *J. Geophys. Res.*, 107, LBA 25-1–LBA 25-11, doi:10.1029/2001JD000358,  
864 2002.

865 Vandaele, A.C. Hermans, C. Simon, P.C. Rozendael, M. Carleer, J.M. and Colin, R.: Fourier  
866 transform measurement of NO<sub>2</sub> absorption cross-section in the visible range at room  
867 temperature, *J. Atmos. Chem.*, 25, 289-305, 1996.

868 Volkamer, R., Spietz, P., Burrows, J., Platt, U.: High-resolution absorption cross-sections of  
869 glyoxal in the UV-vis and IR spectral ranges, *Journal of Photochemistry and Photobiology  
870 A: Chemistry*, 172 (1), 35-46, 2005.

871 Wagner, T., Ibrahim, O., Shaiganfar, R., Platt, U.: Mobile MAX-DOAS observation of  
872 tropospheric trace gases, *Atmos. Meas. Tech.*, 3, 129-140, 2010.

873 Wagner, T., Beirle, S., Brauers, T., Deutschmann, T., Frieß, U., Hak, C., Halla, J. D., Heue,  
874 K. P., Junkermann, W., Li, X., Platt, U., and Pundt-Gruber, I.: Inversion of tropospheric  
875 profiles of aerosol extinction and HCHO and NO<sub>2</sub> mixing ratios from MAX-DOAS  
876 observations in Milano during the summer of 2003 and comparison with independent data  
877 sets, *Atmos. Meas. Tech.*, 4, 2685-2715, doi:10.5194/amt-4-2685-2011, 2011.

878 Wittrock, F., Oetjen, H., Richter, A., Fietkau, S., Medeke, T., Rozanov, A., Burrows, J. P.:  
879 MAX-DOAS measurements of atmospheric trace gases in Ny-Ålesund – Radiative transfer  
880 studies and their application, *Atmos. Chem. Phys.*, 4, 955–966, 2004.

881 Yang, W. X., Meixner, F. X.: Laboratory studies on the release of nitric oxide from  
882 subtropical grassland soils: the effect of soil temperature and moisture, in: *Gaseous  
883 Nitrogen Emissions from Grasslands*, Wallingford, England, 67–70, 1997.

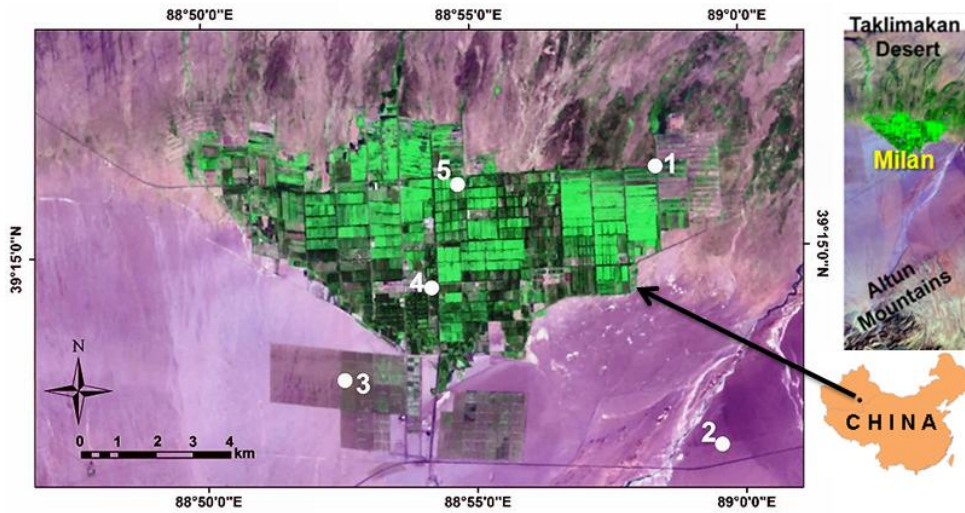
884 [Yamulki, S., Goulding, K.W.T., Webster, C.P. and Harrison, R.M.: Studies on NO and N<sub>2</sub>O  
885 Fluxes from a Wheat Field, \*Atmospheric Environment\*, 29 \(14\), 1627–1635, 1995.](#)

886 Yu, J., Meixner, F. X., Sun, W., Liang, Z., Chen, Y., Mamtimin, B., Wang, G., and Sun, Z.:  
887 Biogenic nitric oxide emission from saline sodic soils in a semiarid region, northeastern  
888 China: a laboratory study, *J. Geophys. Res.*, 113, 1–11, 2008.

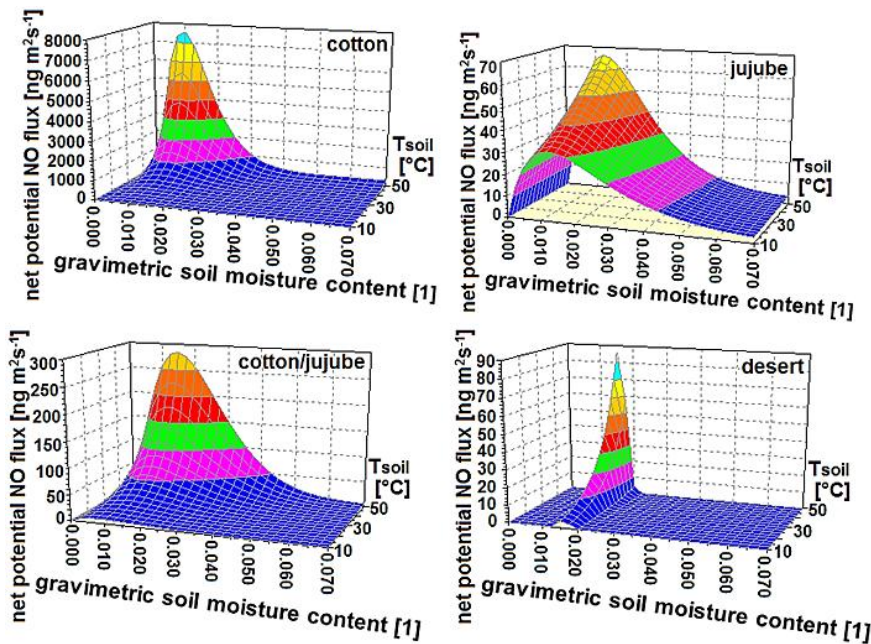
889 Yu, J., Meixner, F. X., Sun, W., Mamtimin, B., Wang, G., Qi, X., Xia, C., and Xie, W.: Nitric  
890 oxide emissions from black soil, northeastern China: a laboratory study revealing  
891 significantly lower rates than hitherto reported, *Soil Biol. Biochem.*, 42, 1784–1792, 2010a.

892 Yu, J., Meixner, F.X., Sun, W., Mamtimin, B., Xia, C., Xie, W.: Biogenic nitric oxide  
893 emission of mountain soils sampled from different vertical landscape zones in the  
894 Changbai Mountains, Northeastern China, *Environ. Sci. Technol.*, 44, 4122–4128, 2010b.  
895

896 **Figures:**

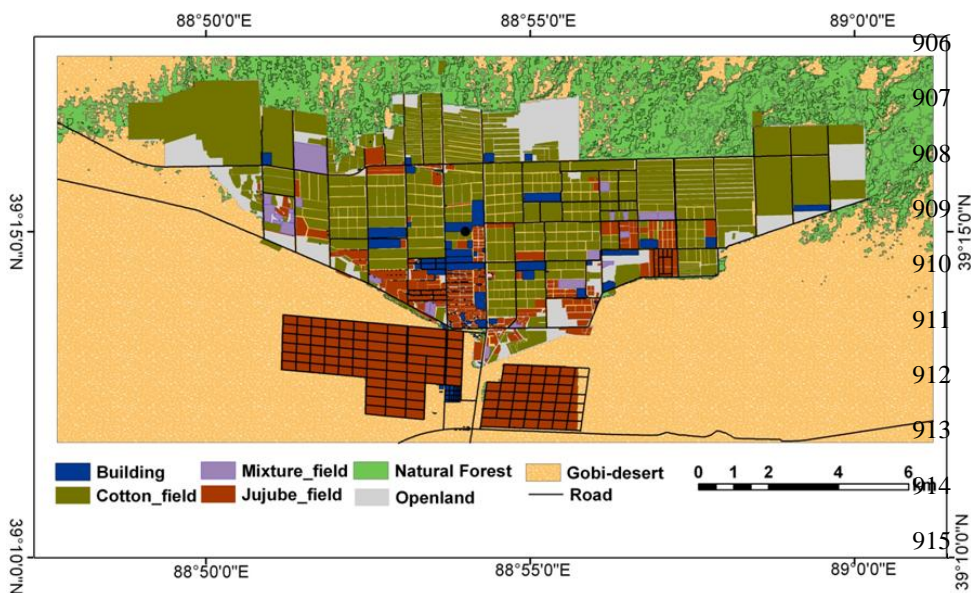


897  
 898 **Fig. 1:** Satellite map (Landsat ETM+; 2011) of Milan oasis, Xinjiang, NW-China (The map  
 899 has an area of 338 km<sup>2</sup>). The white circles show the sites of *in-situ* measurements: natural  
 900 forest (1), desert (2), jujube (3), hotel/oasis station (4) and cotton field (5).

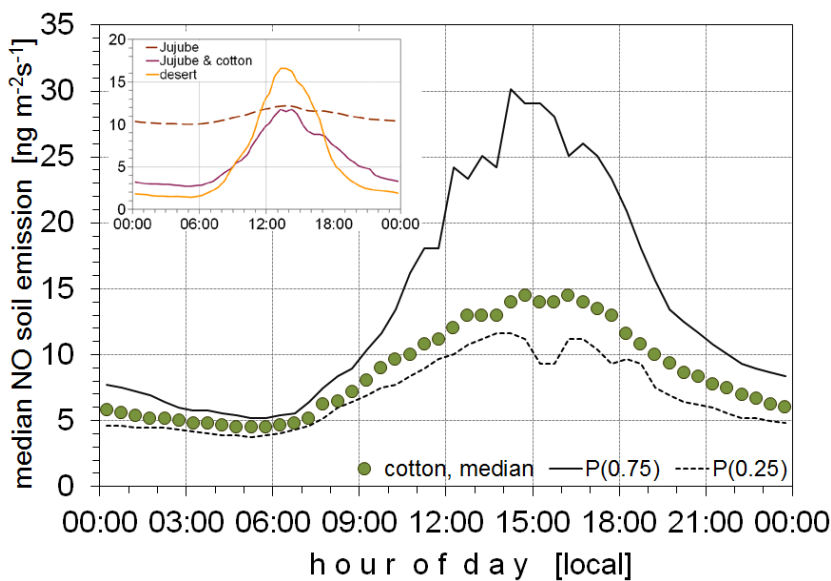


901  
 902 **Fig. 2:** Net potential NO fluxes  $F_{NO}$  ( $\text{ng m}^{-2} \text{s}^{-1}$ ; in terms of mass of nitric oxide) from soils of  
 903 the four major land-cover types of Milan oasis as functions of soil temperature ( $^{\circ}\text{C}$ ) and  
 904 dimensionless gravimetric soil moisture content.

905



916 **Fig. 3:** 2011 map of land-cover types of Milan oasis as derived from satellite images  
 917 (Quickbird, Landsat ETM+, see Sect. 2.2.5).

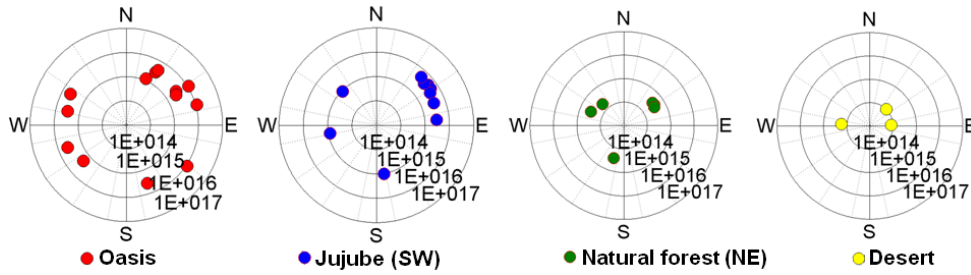


Formatted: Font: Italic

918  
 919 **Fig 4:** median diel variation of the actual NO-flux ( $\text{ng m}^{-2}\text{s}^{-1}$ ; in terms of mass of nitric oxide)  
 920 from soils of the four major land-cover types of Milan oasis for the period 03 to 24 June,  
 921 2011. Data have been calculated according eq.(10) using (a) soil temperatures (medians)  
 922 measured for each of the four major land-cover types, and (b) so-called “wilting point”-data  
 923 for corresponding soil moisture contents at the four sites (s. section 2.2.3). Data for the  
 924 cotton-site are given as medians, as well as 25 and 75% quantiles, those for the Jujube,  
 925 Jujube-cotton and desert sites as medians only (s. figure insert).

926

927



928

929 | **Fig. 5:** Results of MAX-DOAS measurements performed at sites oasis/hotel (4), Jujube (3),  
 930 Natural forest (1), and Desert (2) of Milan oasis from 23 May to 26 June, 2011 (see Fig. 1).  
 931 Vertical  $\text{NO}_2$  column densities (in molecules  $\text{cm}^{-2}$ ; 20-30 min averages) are shown in relation  
 932 to in-situ measured wind direction at each location of MAX-DOAS measurements. The  
 933 MAX-DOAS measurements were performed between 6:00 and 19:00 (local time). Note the  
 934 radial logarithmic scale of VCD data.

935

936

937

938

939

940

941

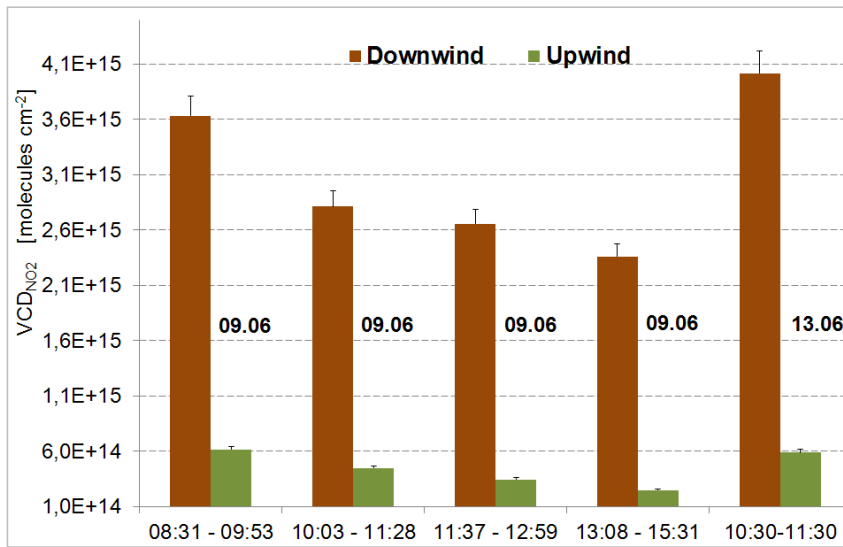
942

943

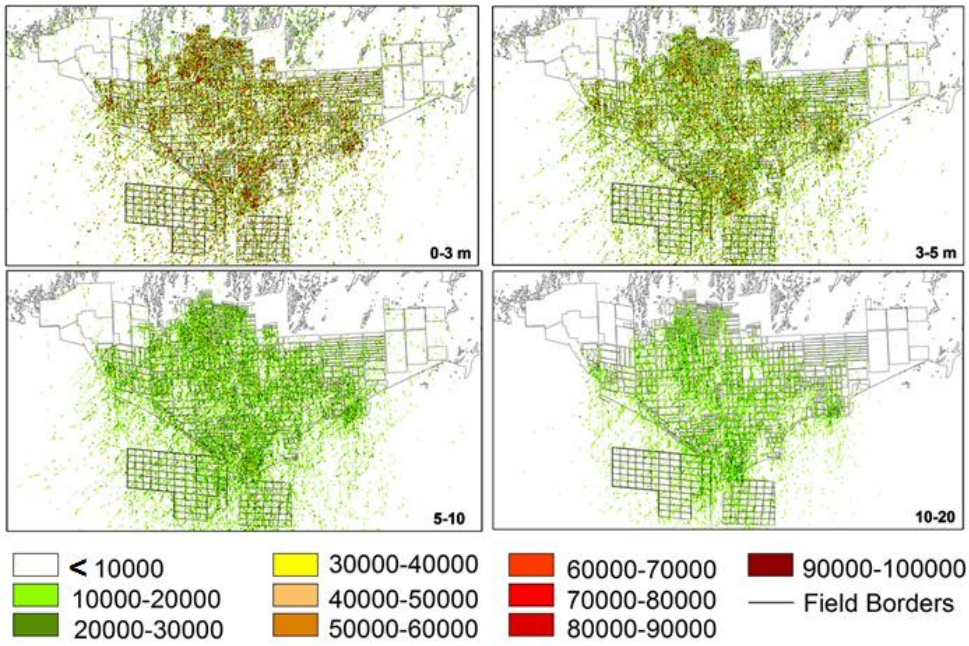
944

945

946



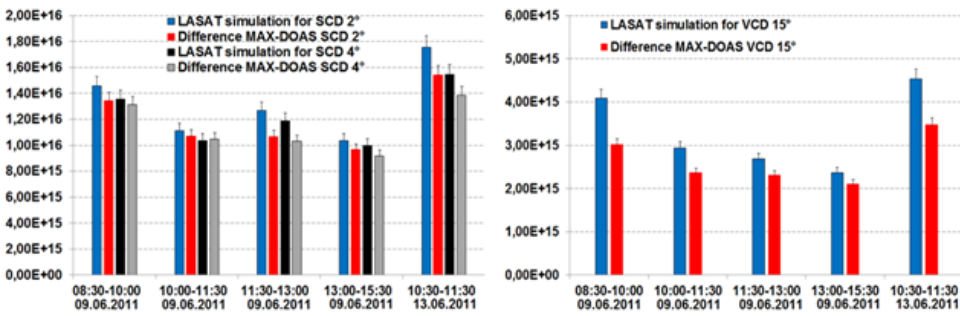
947 | **Fig. 6:** Results of  $\text{NO}_2$ -VCD measured simultaneously with two MAX-DOAS instruments up-  
 948 wind (natural forest, site (1)) and downwind (jujube field, site (3)) of Milan oasis on 09 and  
 949 13 June, 2011.



950

951 **Fig. 7:** Results of NO concentrations ( $\text{ng m}^{-3}$ ; in terms of mass of nitric oxide) calculated by  
 952 the LASAT dispersion model for the first four vertical levels on 09 June, 2011, 11:30 to 13:00  
 953 (local time).

954



955

956 **Fig. 8:** Simulated SCDs vs. SCDs measured by MAX-DOAS (a) and simulated VCDs vs.  
 957 VCDs measured by MAX-DOAS (b) on 09 and 13 June, 2011 at Milan oasis. SCDs have  
 958 been measured and simulated for elevation angles of  $2^\circ$  and  $4^\circ$ , VCDs were measured at  $15^\circ$ .

959

960